Editors' Suggestion

Applicability of Eliashberg theory for systems with electron-phonon and electron-electron interaction: A comparative analysis

Shang-Shun Zhang, Zachary M. Raines, and Andrey V. Chubukov
School of Physics and Astronomy and William I. Fine Theoretical Physics Institute, University of Minnesota, Minneapolis, Minnesota 55455, USA

(Received 17 April 2024; revised 30 May 2024; accepted 31 May 2024; published 24 June 2024)

We present a comparative analysis of the validity of Eliashberg theory for the cases of fermions interacting with an Einstein phonon and with soft nematic fluctuations near an Ising-nematic/Ising-ferromagnetic quantum-critical point (QCP) in two spatial dimensions. In both cases, Eliashberg theory is obtained by neglecting vertex corrections. For the phonon case, the reasoning to neglect vertex corrections is the Migdal "fast electron/slow boson" argument because the phonon velocity is much smaller than the Fermi velocity, v_F. The same argument allows one to compute the fermionic self-energy within Eliashberg theory perturbatively rather than self-consistently. For the nematic case, the velocity of a collective boson is comparable to v_F and this argument does not work. Nonetheless, we argue that while two-loop vertex corrections near a nematic QCP are not small parametrically, they are small numerically. At the same time, perturbative calculation of the fermionic self-energy can be rigorously justified when the fermion-boson coupling is small compared to the Fermi energy by effectively invoking the fast electron/slow boson argument, this time because bosons are Landau overdamped. Furthermore, we argue that for the electron-phonon case Eliashberg theory breaks down at some distance from where the dressed Debye frequency would vanish, while for the nematic case it holds all the way to a QCP. From this perspective, Eliashberg theory for the nematic case actually works better than for the electron-phonon case.

DOI: 10.1103/PhysRevB.109.245132

I. INTRODUCTION

Migdal-Eliashberg (ME) theory has been developed to describe electron-phonon interaction in the normal state and phonon-induced superconductivity [1,2]. Over the years, it has been successfully applied to numerous electron-phonon systems [3–8]. The theory, as formulated by Eliashberg [2], consists of a set of three coupled self-consistent one-loop equations for the normal and anomalous fermionic self-energies and the phonon polarization. These equations can be derived either diagrammatically or from the variational Luttinger-Ward functional [9], assuming that vertex corrections can be neglected. ME argued that vertex corrections are small in the ratio of the dressed Debye frequency ω_D to the Fermi energy E_F. The physical reasoning, due to Migdal [1], is that in processes leading to vertex corrections a fermion is forced to vibrate at the phonon frequency, which for small ω_D/E_F is far from its own resonance. In mathematical terms, the strength of vertex corrections is governed by the dimensionless Eliashberg parameter $\lambda_E = g^2/(\omega_D E_F)$, where g is an effective fermion-boson interaction, which we define below (it depends on the bare Debye frequency $\omega_{D,0}$, but *not* on the dressed ω_D). The parameter λ_E is different from the dimensionless coupling $\lambda = g^2/\omega_D^2$, which determines mass renormalization: $\lambda_E = \lambda(\omega_D/E_F) \ll \lambda$. By this reasoning, the one-loop theory remains under control not only at weak coupling, where $\lambda < 1$, but also at strong coupling, where $\lambda > 1$, as long as $\lambda_E < 1$ [i.e., at $\omega_D < g < (\omega_D E_F)^{1/2}$]. Still, when the Debye frequency softens, λ_E eventually becomes large and the one-loop description breaks down. At larger λ_E, higher loop processes become relevant and eventually lead to a polaronic description.

In recent years, a similar description has been applied to metals in which electron-electron interaction (screened Coulomb repulsion) gives rise to long-range particle-hole order either in the spin or charge channel [10–42]. Near the onset of such an order, i.e., near a quantum-critical point (QCP), it is natural to assume that the low-energy physics is described by an effective model with fermion-fermion interactions mediated by soft fluctuations of the bosonic order parameter that condenses at the QCP. The theory near a QCP is based on the same set of coupled equations that Eliashberg obtained for the electron-phonon case and bears his name.

The validity of Eliashberg theory for a system near a QCP has been questioned, however, on the grounds that the "fast fermion/slow boson" argument, used to justify the neglect of vertex corrections, is not applicable anymore because collective excitations are made out of fermions and their velocity is of order v_F (see, e.g., Ref. [43]). The counterargument [19] is that soft collective excitations are Landau overdamped and for this reason do behave as slow modes compared to fermions, i.e., Migdal's reasoning is still valid, albeit for a different reason.

The aim of this paper is to settle the issue of applicability of the Eliashberg (one-loop) theory for a quantum-critical metal near a QCP. We compare the criteria for applicability of the Eliashberg theory for fermions interacting with a soft Einstein phonon with $\omega_D \ll E_F$ and with soft nematic fluctuations near an Ising-nematic/Ising-ferromagnetic QCP. We argue that the

criteria for these two cases are somewhat similar, but not identical.

Below we focus on the case of two spatial dimensions (2D) and restrict our analysis to the normal state at $T = 0$. This is a putative ground state as the true one is a superconductor in both cases. However, for spin-singlet pairing, the criterion for validity of the Eliashberg theory for a superconductor is actually weaker than that for the normal state as singular quantum corrections to the self-energy cancel in the gap equation like contributions from nonmagnetic impurities [15,44,45]. For this reason, if ME theory is applicable in the putative normal state, it is also applicable to a superconductor. Restriction to $T = 0$ is essential because thermal fluctuations do not fit into ME reasoning and may destroy ME theory at a finite T faster than quantum fluctuations at $T = 0$ (see Refs. [8,46] for more detail).

We also do not discuss here logarithmic singularities in the fermionic self-energy in the Ising-nematic/Ising-ferromagnetic case that emerge at three-loop and higher orders [47–50]. Most likely, these corrections generate an anomalous dimension for the fermionic propagator, but the branch cut in the Green's function remains at the same place as in the Eliashberg theory.

Finally, for the electron-phonon case, we do not discuss here the proposals [51–54] that the transition to polarons may be first order and happen already at $\lambda = O(1)$ due to singular behavior of n-loop contributions to the self-energy with $n \gg 1$ (Ref. [54]). In this paper we restrict the analysis of the self-energy to two-loop order.

A. Summary of the results

As we said above, for the electron-phonon case, the smallness of vertex corrections to the electron self-energy is controlled by the Eliashberg parameter $\lambda_E = g^2/(\omega_D E_F) = \lambda\omega_D/E_F$. This parameter is small at weak coupling, when $\lambda < 1$, but remains small also at strong coupling, $\lambda > 1$, as long as $\lambda < E_F/\omega_D$. At larger λ vertex corrections become parametrically large and Eliashberg theory breaks down. This happens at a finite ω_D, unless one takes the double limit $E_F \to \infty$ and $\omega_D \to 0$ while maintaining $g^2 \ll \omega_D E_F$ [45,55]. If E_F is kept finite, as we do in this paper, $\lambda_E = O(1)$ is reached at a finite ω_D.

For the Ising-nematic/Ising-ferromagnetic case, vertex corrections are small at weak coupling, when the corresponding λ^*, defined via $\lambda^* = \lim_{\omega_m \to 0} \partial\Sigma/\partial\omega_m$, is small. In the strong coupling regime $\lambda^* > 1$, vertex corrections are not small parametrically. However, they remain of order one and are small numerically (of order 10^{-2}). This behavior holds all the way up to the QCP, where vertex corrections remain numerically small.

There is more. The two Eliashberg equations for the dynamical fermionic self-energy and bosonic polarization, obtained from the Luttinger-Ward functional, are coupled self-consistent one-loop equations. The one for the bosonic polarization accounts for Landau damping of the bosons. For the electron-phonon case the *same* parameter $\lambda_E < 1$ that justifies the neglect of vertex corrections also allows one to simplify these equations in the following way: (i) neglect the Landau damping, (ii) neglect momentum dependence of $\Sigma(k)$, i.e., approximate $\Sigma(k)$ by $\Sigma(\omega_m)$, and (iii) replace the self-consistent one-loop equation for $\Sigma(\omega_m)$ by the perturbative one-loop formula, in which the self-energy is expressed in terms of the bare fermionic propagator. We argue that these simplifications are possible because typical fermionic momenta transverse to the Fermi surface are small compared to typical momenta along the Fermi surface ($\lambda_E k_F$ vs k_F).

For the Ising-nematic/Ising-ferromagnetic case, Landau damping is relevant but $\Sigma(k)$ can again be replaced by $\Sigma(\omega_m)$ and the self-consistent one-loop Eliashberg equations can be still reduced to the perturbative ones. This happens because typical momenta transverse to the Fermi surface are again smaller than typical momenta along the Fermi surface. This smallness holds in λ_E^*, which is the ratio of the fermion-boson coupling and the Fermi energy. This ratio must be small, as otherwise the low-energy description would not be valid. The value of λ_E^* does not depend on the distance to the QCP and hence for the Ising-nematic/Ising-ferromagnetic case the one-loop perturbation theory remains valid even at the critical point.

The outcome of this analysis is the following. For the electron-phonon case, the condition $\lambda_E < 1$ allows one to rigorously neglect vertex corrections to Eliashberg theory and at the same time simplifies the calculations within Eliashberg theory, e.g., allows one to compute the fermionic self-energy in one-loop perturbation theory rather than self-consistently. Because λ_E is inversely proportional to ω_D, both Eliashberg theory and approximate treatment within it are valid only at ω_D above some critical value.

For the Ising-nematic/Ising-ferromagnetic case, Eliashberg theory is not rigorously justified at strong coupling, but vertex corrections remain $O(1)$ and are small numerically even at a QCP. At the same time, there exists another small parameter λ_E^* (the ratio of the interaction to the Fermi energy), which justifies the computation of the fermionic self-energy within Eliashberg theory in a perturbative one-loop analysis rather than self-consistently. This parameter also remains small at a QCP.

From this perspective, Eliashberg theory near a Ising-nematic/Ising-ferromagnetic QCP actually works better than for fermions interacting with a soft Einstein phonon, despite the fact that the velocity of collective bosons is of order v_F.

The structure of the paper is the following. In the next section we briefly review Eliashberg theory for electron-phonon interaction [2,7,8] and discuss the strength of one-loop vertex corrections. In Sec. III we discuss fermions near a nematic QCP. In Sec. IV we compare the two cases and present our conclusions.

II. ELIASHBERG THEORY FOR ELECTRON-PHONON SYSTEM

For definiteness, we consider interaction with an Einstein phonon; qualitatively similar considerations apply for acoustic phonons, but the functional form of the self-energy and vertex corrections will differ from that presented below. The Hamiltonian has a standard form: $\mathcal{H} = \mathcal{H}_{\text{el}} + \mathcal{H}_{\text{ph}} + \mathcal{H}_{el\text{-ph}}$, where $\mathcal{H}_{\text{el}}$ describes free electrons with dispersion $\epsilon_{\mathbf{k}}$, $\mathcal{H}_{\text{ph}}$ describes a phonon with a bare Debye frequency $\omega_{D,0}$, and $\mathcal{H}_{el\text{-ph}} = \tilde{g}\sum_{i,\sigma}(c^\dagger_{i,\sigma}c_{i,\sigma} + \text{H.c.})(a^\dagger_i + a_i)$, where $a^\dagger_i, a_i$ are

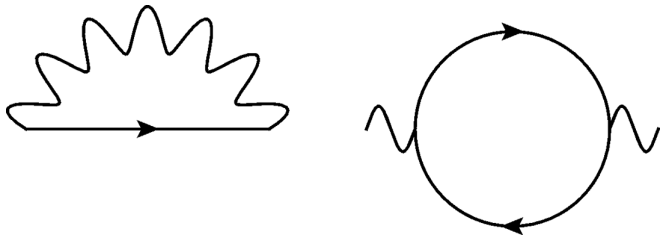

FIG. 1. Self-consistent one-loop electron self-energy (left panel) and polarization bubble for Einstein phonon (right panel). Solid lines indicate the renormalized electronic Green's function $G(k)$ and wavy lines the renormalized Einstein phonon propagator $\chi(q)$.

creation and annihilation operators of a phonon at site i, $c^{\dagger}_{I,\sigma}$, $c_{I,\sigma}$ are creation and annihilation operators of an electron with spin polarization σ at site i, and $\tilde{g}$ is the electron-phonon coupling with dimension energy over momentum.

Eliashberg theory for the normal state consists of the set of two equations for the fermionic self-energy $\Sigma(k)$ and phonon polarization $\Pi(q)$, where $k \equiv (\mathbf{k}, \omega)$ and $q \equiv (\mathbf{q}, \Omega)$. The equations look simplest along the Matsubara axis where $\omega = \omega_m = (2m+1)\pi T$ and $\Omega = \Omega_n = 2n\pi T$. The full fermionic Green's function and the full phonon propagator are related to Σ and Π via

$$G^{-1}(k) = G_0^{-1}(k) + i\Sigma(k), \quad \chi^{-1}(q) = \chi_0^{-1}(q) + \Pi(q), \tag{1}$$

where $G_0(k)$ and $\chi_0(q)$ are electron and phonon propagators in the absence of interaction. We include a factor of i in the definition of Σ for notational convenience.

In analytical form

$$G_0(k) = \frac{1}{i\omega_m - \epsilon_{\mathbf{k}}}, \quad \chi_0(q) = \frac{D_0}{\Omega_n^2 + \omega_{D,0}^2}, \tag{2}$$

where $D_0 = 2\omega_{D,0}$. Note that $\chi_0(q)$ has dimension of inverse energy. For purely local self-energy, $\Sigma(k) = \Sigma(\omega_m)$ and $G^{-1}(k) = i[\omega_m + \Sigma(\omega_m)] - \epsilon_{\mathbf{k}}$.

The self-consistent equations for Σ and Π can be either derived diagrammatically, see Fig. 1, or obtained as stationary solutions of the Luttinger-Ward functional. Along the Matsubara axis, they are

$$\Sigma(k) = i\tilde{g}^2 \int \frac{d^2\mathbf{q}\, d\Omega_n}{(2\pi)^3} G(k+q)\chi(q), \tag{3}$$

$$\Pi(q) = 2\tilde{g}^2 \int \frac{d^2\mathbf{k}\, d\omega_m}{(2\pi)^3} G(k+q)G(k). \tag{4}$$

To simplify calculations, we assume a parabolic dispersion, $\epsilon_{\mathbf{k}} = (\mathbf{k}^2 - k_F^2)/(2m)$. At $T = 0$, which we consider here, both ω_m and Ω_n are continuous variables. We also split $\Pi(q)$ into static and dynamic parts and incorporate the static part into $\chi_0(q)$. We assume that the momentum dependence of static $\Pi(q)$ can be neglected, in which case static $\Pi(q)$ renormalizes bare $\omega_{D,0}$ into dressed ω_D. We then redefine $\chi_0(q)$ as

$$\chi_0(q) = \frac{2\omega_{D,0}}{\Omega_n^2 + \omega_D^2}. \tag{5}$$

We will consider the regime in which ω_D gets progressively smaller, but $\omega_{D,0}$ remains finite. We will also introduce, instead of $\tilde{g}$, the effective interaction with dimension of energy $g = (\tilde{g}^2 N_F D_0)^{1/2}$, where $N_F = k_F/(2\pi v_F)$ is the density of states at the Fermi level per spin component. We emphasize that g depends on the bare Debye frequency rather than the dressed one, ω_D. We therefore consider g and ω_D as independent variables.

Out of ω_D, g, and the Fermi energy $E_F = k_F^2/(2m)$, one can introduce two dimensionless ratios

$$\lambda = \frac{g^2}{\omega_D^2}, \quad \lambda_E = \frac{g^2}{E_F \omega_D} = \lambda \frac{\omega_D}{E_F}. \tag{6}$$

Eliashberg theory is constructed under the assumptions that E_F is the largest energy scale and $\lambda_E \ll \lambda$. The ME argument is that the strength of vertex corrections is determined by the smaller λ_E, while fermionic mass renormalization is determined by the larger λ. When both λ and λ_E are small, the theory falls into the weak coupling limit with G and χ close to their bare expressions. In the regime $\lambda > 1$, $\lambda_E < 1$, the mass renormalization is large and the self-energy is larger than bare ω_m over a wide range of frequencies, yet vertex corrections are still small.

We will be chiefly interested in the strong coupling regime $\lambda > 1$, $\lambda_E < 1$. We go beyond previous work [8] and analyze vertex corrections in 2D for all phonon momenta. We also compute the two-loop self-energy with vertex correction included. We show that the latter is small in λ_E and becomes $O(1)$ when $\lambda_E \sim 1$.

ME found [1,2] that the same small parameter λ_E allows one to simplify calculations within Eliashberg theory and obtain a simple expression for the self-energy, $\Sigma^{(E)}(\omega_m) = \lambda\omega_D \arctan(\omega_m/\omega_D)$ [Eq. (13) below], which depends only on frequency. Here we analyze the corrections to this expression, both analytically and numerically. We show that Eq. (13) can be rigorously justified only for frequencies $\omega_m \ll E_F$. At $\omega_m \sim E_F$, the expression is more complex [Eq. (14) below]. In particular, $\Sigma(k_F, \omega_m)$ becomes complex on the Matsubara axis,[1] similar to the self-energy in SYK-type models [56,57].

We also show that the momentum-dependent part of the self-energy remains small as long as $\lambda_E < 1$. In the remainder of this section, we first discuss the solution of the Eliashberg equations and then use it to analyze the strength of vertex corrections.

A. Solution of Eliashberg equations

The equations for $\Sigma(k)$ and $\Pi(q)$ are coupled and in principle have to be solved together. We argue, however, that for $\lambda_E \ll 1$ the two equations can be solved independently. To demonstrate this, we make two assumptions and verify both *a posteriori*. First, we assume that $\partial\Sigma(k)/\partial\omega_m$ scales as λ and is large at strong coupling, while $\partial\Sigma(k)/\partial\epsilon_{\mathbf{k}}$ scales as λ_E and is small when $\lambda_E < 1$. Accordingly, we approximate $\Sigma(\mathbf{k}, \omega_m)$ by $\Sigma(\omega_m)$. Second, we assume that $\Sigma(\omega_m)$ is parametrically smaller than E_F.

[1]This does not violate Kramers-Kronig relations, but when $\Sigma(k_F, \omega_m)$ is complex, both $\Sigma'(k_F, \omega)$ and $\Sigma''(k_F, \omega)$ on the real axis have even and odd components in ω.

Consider Eq. (4) for $\Pi(q)$ first. Like we said, we express $\Pi(q) = \Pi(\mathbf{q}, \Omega_n)$ as a sum of static and dynamic pieces $\Pi(\mathbf{q}, 0) + \delta\Pi(\mathbf{q}, \Omega_n)$ and incorporate the static part $\Pi(\mathbf{q}, 0)$ into a redefinition of $\chi_0(q)$. The static polarization generally comes from high-energy fermions with excitation energies of order E_F. It renormalizes $\omega_{D,0}$ into the dressed ω_D and may also give rise to a momentum dependence of the phonon propagator. For the purposes of this study we assume that the momentum dependence induced by $\Pi(\mathbf{q}, 0)$ is weak and does not affect the physics at small but still finite ω_D, which we consider here (for more discussions on this issue, see Refs. [58] and [8]). The second, dynamical term comes from fermions with low energies, comparable to Ω_n. For this term we obtain, after integrating over the angle between phonon $\mathbf{q}$ and fermionic $\mathbf{k}$,

$$\delta\Pi(q) = -2i\tilde{g}^2 \int \frac{d\omega_m}{2\pi} \int \frac{k\,dk}{2\pi} \frac{1}{i\tilde{\Sigma}(\omega_m) - \epsilon_{\mathbf{k}}} \left[\frac{\mathrm{sgn}(\omega_m + \Omega_n)}{\sqrt{\frac{(kq)^2}{m^2} + \left[\tilde{\Sigma}(\omega_m + \Omega_n) + i\left(\epsilon_{\mathbf{k}} + \frac{q^2}{2m}\right)\right]^2}} - \text{the same at } \Omega_n = 0 \right], \tag{7}$$

where for brevity we have defined $\tilde{\Sigma}(\omega_m) = \omega_m + \Sigma(\omega_m)$. For $\omega_m, \Omega_n \ll E_F$ and a generic $q \sim k_F$, the terms $\tilde{\Sigma}(\omega_m + \Omega_n)$ and $\epsilon_{\mathbf{k}}$ under the square root in Eq. (7) are much smaller than E_F and can be neglected compared to the two q-dependent terms, which are of order E_F. Equation 7 then simplifies to

$$\delta\Pi(q) = -2i\tilde{g}^2 N_F \int \frac{d\omega_m}{2\pi} \int \frac{d\epsilon_{\mathbf{k}}}{i\tilde{\Sigma}(\omega_m) - \epsilon_{\mathbf{k}}} \times \frac{\mathrm{sgn}(\omega_m + \Omega_n) - \mathrm{sgn}(\omega_m)}{v_F q \sqrt{1 - (q/2k_F)^2}}, \tag{8}$$

where N_F is the density of states at the Fermi level per spin component. Integration over $\epsilon_{\mathbf{k}}$ can now be extended to infinite limits [up to terms of order $\tilde{\Sigma}(\omega_m)/E_F \ll 1$] and yields $\int d\epsilon_{\mathbf{k}}/[i\tilde{\Sigma}(\omega_m) - \epsilon_{\mathbf{k}}] = -i\pi\,\mathrm{sgn}(\omega_m)$. Integrating then over frequency, we obtain

$$\delta\Pi(q) = 2\tilde{g}^2 N_F \frac{\Omega_n}{v_F q \sqrt{1 - (q/2k_F)^2}}. \tag{9}$$

This expression is valid only for $q < 2k_F$, which is the largest momentum transfer on the Fermi surface. At small q, it reduces to conventional Landau damping. Substituting $\delta\Pi$ into Eq. (1) and using Eq. (2), we obtain

$$\chi(\mathbf{q}, \Omega_n) = \frac{D_0}{\Omega_m^2 + \omega_D^2 + \gamma \frac{|\Omega_n|}{q\sqrt{1-(q/2k_F)^2}}}, \tag{10}$$

where $\gamma = 2g^2/v_F$ and, we remind, $g^2 = \tilde{g}^2 N_F D_0$.

It is convenient to measure q in units of $2k_F$ and Ω_n in units of ω_D. Introducing $\bar{q} = q/(2k_F)$ and $\bar{\Omega}_n = \Omega_n/\omega_D$, we reexpress Eq. (10) as

$$\chi(\mathbf{q}, \Omega_n) = \frac{D_0}{\omega_D^2} \frac{1}{1 + \bar{\Omega}_n^2 + \frac{\lambda_E}{2} \frac{|\bar{\Omega}_n|}{\bar{q}\sqrt{1-\bar{q}^2}}}. \tag{11}$$

We see that the Landau damping term contains λ_E in the prefactor and is therefore small compared to one of the two other terms for all values of $\bar{\Omega}_n$ provided that $\bar{q}$ is not close to either zero or one.

We now substitute $\chi(\mathbf{q}, \Omega_n)$ from Eq. (11) into Eq. (3) for the self-energy. We compute separately $\Sigma(\mathbf{k}_F, \omega_m)$ and $\Sigma(\mathbf{k}, 0)$. The calculation of $\Sigma(\mathbf{k}_F, \omega_m)$, which we denote as $\Sigma(\omega_m)$ for brevity, parallels the one for $\delta\Pi$: we first integrate over the angle between $\mathbf{k}_F$ and $\mathbf{q}$ and obtain

$$\Sigma(\omega_m) = \frac{g^2}{N_F} \int \frac{d\Omega_n}{2\pi} \int_0^{2k_F} \frac{q\,dq}{2\pi} \frac{1}{\Omega_n^2 + \omega_D^2 + \gamma \frac{|\Omega_n|}{q\sqrt{1-(q/2k_F)^2}}} \times \frac{\mathrm{sgn}(\omega_m + \Omega_n)}{\sqrt{(v_F q)^2 + \left(\tilde{\Sigma}(\omega_m + \Omega_n) + i\frac{q^2}{2m}\right)^2}}. \tag{12}$$

We set $\omega_m \ll E_F$ and assume and verify a posteriori that (i) typical q are of order k_F and typical Ω_n are of order ω_m and (ii) $\tilde{\Sigma}(\omega_m + \Omega_n)$ is parametrically smaller than E_F. We then evaluate the integrals over q and Ω_n neglecting the Landau damping term and $\tilde{\Sigma}(\omega_m + \Omega_n)$ under the square root. The calculation is elementary and we obtain

$$\Sigma^{(E)}(\omega_m) = \lambda\omega_D \arctan\left(\frac{\omega_m}{\omega_D}\right), \tag{13}$$

where the index E denotes that this is the leading self-energy in Eliashberg theory. The self-energy behaves as $\lambda\omega_m$ at small frequencies and saturates at higher frequencies at $(\pi/2)\lambda\omega_D \mathrm{sgn}\omega_m$. We emphasize that Eq. (13) has been obtained by neglecting the self-energy of an intermediate fermion and therefore has the same form as if we used the Green's function for free fermions. The same holds for $\delta\Pi(q)$. In other words, to this accuracy, the one-loop self-consistent theory becomes equivalent to the one-loop perturbation theory. We plot $\Sigma^{(E)}(\omega_m)$ in Fig. 2 for $\omega_m > 0$. The self-energy exceeds the bare ω_m at $\omega_m < \omega_c$, where $\omega_c \equiv (\pi/2)\lambda\omega_D = (\pi/2)\lambda_E E_F$, and becomes smaller than ω_m at higher frequencies. As long as λ_E is small, ω_c is parametrically smaller than E_F.

We next check the accuracy of approximations used to obtain Eq. (13). One can straightforwardly verify that typical q for the momentum integral are of order k_F and typical Ω_n for the frequency integral are of order ω_m, as we assumed. Further, the prefactor $\lambda\omega_D$ in Eq. (13) can be equivalently expressed as $\lambda_E E_F$. We see that for small λ_E, $\tilde{\Sigma}(\omega_m + \Omega_n) \ll E_F$, which is the value for a typical $v_F q$. This justifies neglecting the self-energy term in Eq. (12) and in the calculation of $\delta\Pi(q)$.

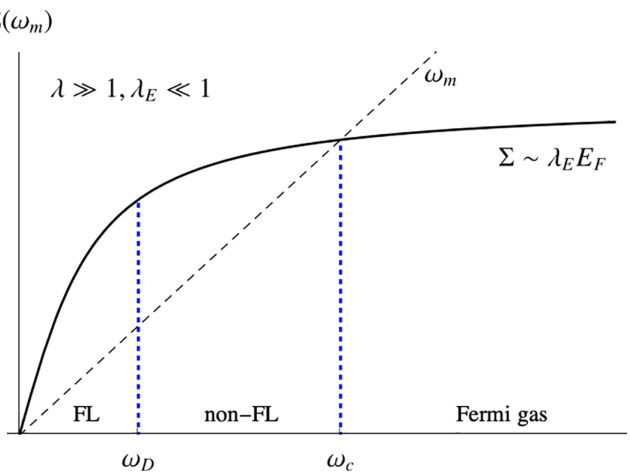

FIG. 2. One-loop perturbative Eliashberg self-energy $\Sigma^{(E)}(\omega_m)$ at $\lambda \gg 1$, but $\lambda_E \ll 1$. The self-energy is linear in ω_m for $\omega_m < \omega_D$ and saturates at larger ω_m. It is larger than the bare ω_m for $\omega_m < \omega_c \equiv (2/\pi)E_F\lambda_E$. For $\omega_m < \omega_D$, the system is in the Fermi liquid regime. In between ω_D and ω_C, it displays strong coupling, non-Fermi liquid behavior. At larger ω_m the self-energy is smaller than ω_m and the system behaves as a Fermi gas.

B. Subleading terms in the self-energy

We now go beyond the leading term and estimate the subleading terms in the self-energy. They are the corrections to the dynamic piece of the self-energy, arising from keeping the Landau damping term and $\tilde{\Sigma}$ in the right-hand side of Eq. (12) and the static piece of the self-energy $\Sigma(\mathbf{k}, 0)$. Keeping the Landau damping term in Eq. (12) leads to a relative correction $1 + X(\omega_m)$, which is the largest at $\omega_m \sim \omega_D$, where $X \sim \lambda_E \log^2 \lambda_E$. This is a small correction when $\lambda_E \ll 1$. The leading correction from keeping $\tilde{\Sigma}(\omega_m + \Omega_n)$ in the integrand in Eq. (12) comes from $q \approx 2k_F$. We label this correction as $\delta\Sigma(\omega_m)$. Calculation shows that $\delta\Sigma(\omega_m)$ is a complex function of Matsubara frequency. Similar behavior of $\Sigma(\omega_m)$ has been previously reported in SYK-type systems [56,57]. In our case the appearance of a complex $\Sigma(\omega_m)$ reflects the absence of particle-hole symmetry for a parabolic dispersion. At $|\omega_m| < \omega_D$, the real part of $\delta\Sigma(\omega_m)$ is linear in ω_m, like $\Sigma^{(E)}(\omega_m)$, but with the prefactor $\lambda\sqrt{\lambda_E}$, which is smaller than that in Eq. (13) by $\sqrt{\lambda_E}$. For $\omega_D < |\omega_m| < E_F$,

$$\delta\Sigma(\omega_m) = -\omega_c \left(\frac{|\tilde{\Sigma}^{(E)}(\omega_m)|}{E_F} \right)^{1/2} \frac{1 + i\,\mathrm{sgn}\omega_m}{\pi}. \tag{14}$$

Substituting $|\tilde{\Sigma}^{(E)}(\omega_m)| \approx |\omega_m| + \omega_c$, we find that for $|\omega_m| < \omega_c$, $\delta\Sigma(\omega_m)$ is smaller than $\Sigma^{(E)}$ by $(\omega_c/E_F)^{1/2} \sim \lambda_E^{1/2}$. At larger frequencies, $\delta\Sigma$ increases and at $\omega_m \sim E_F$ becomes of the same order as $\Sigma^{(E)}(\omega_m)$. We emphasize that this holds even when λ_E is small. At even larger $|\omega_m| > E_F$, the full self-energy has to be reevaluated. We will not analyze this frequency range here.

The computation of the static piece $\Sigma(\mathbf{k}, 0)$ proceeds in the same way as the computation of of $\Sigma(k_F, \omega_m)$. After angular integration, the static part of Eq. (3) becomes

$$\Sigma(\mathbf{k}, 0) = \frac{g^2}{N_F} \int \frac{d\Omega_n}{2\pi} \int_0^{2k_F} \frac{q\,dq}{2\pi} \frac{1}{\Omega_n^2 + \omega_D^2 + \gamma \frac{|\Omega_n|}{q\sqrt{1-(q/2k_F)^2}}} \times \frac{\mathrm{sgn}(\Omega_n)}{\sqrt{(v_F q)^2 + \left[\tilde{\Sigma}(\Omega_n) + i\left(\epsilon_{\mathbf{k}} + \frac{q^2}{2m}\right)\right]^2}}. \tag{15}$$

Expanding in $\epsilon_{\mathbf{k}}$, we obtain

$$i\Sigma(\mathbf{k}, 0) = \epsilon_{\mathbf{k}} \frac{2g^2}{N_F} \int \frac{d\Omega_n}{2\pi} \int_0^{2k_F} \frac{q\,dq}{2\pi} \frac{1}{\Omega_n^2 + \omega_D^2 + \gamma \frac{|\Omega_n|}{q\sqrt{1-(q/2k_F)^2}}} \times \frac{|\tilde{\Sigma}(\Omega_n)|}{[\tilde{\Sigma}^2(\Omega_n) + (v_F q)^2[1 - (q/2k_F)^2]]^{3/2}}. \tag{16}$$

The largest contributions to the momentum integral come from small q and from $q \approx 2k_F$. Evaluating the contributions from these two regions and performing the subsequent integration over frequency, we obtain

$$i\Sigma(\mathbf{k}, 0) = \lambda_E \epsilon_{\mathbf{k}}. \tag{17}$$

As a consequence, the $\epsilon_{\mathbf{k}}$ term in the bare Green's function gets multiplied by the factor $1 - \lambda_E$. This renormalization is small when λ_E is small.

Summarizing, we find that the condition $\lambda_E \ll 1$ allows us to (i) neglect the Landau damping term in the bosonic propagator, (ii) neglect the momentum dependence of the self-energy, and (iii) approximate $\Sigma(\omega_m)$ by the one-loop perturbative result Eq. (13). For the latter, the corrections, which make $\Sigma(\omega_m)$ complex, are parametrically small as long as ω_m remains below $\omega_c \sim \lambda_E E_F$. At larger frequencies, the corrections get stronger and at $\omega_m \sim E_F$ become of the same order as $\Sigma^{(E)}(\omega_m)$. To the best of our knowledge, this last result has not been presented earlier.

The smallness of corrections to the one-loop perturbative $\Sigma^{(E)}(\omega_m)$ can be understood by comparing relative energy scales and invoking the argument about slow phonons and fast electrons, which typically is reserved for vertex corrections. Indeed, the argument implies that, for the same frequency, fermionic momenta are far smaller than phonon momenta. In our case, typical phonon momenta are of order k_F, while typical fermionic momenta are of order $\tilde{\Sigma}(\omega_m)/v_F$. For $|\omega_m| < \omega_c$, where Eq. (13) for $\Sigma^{(E)}(\omega_m)$ is rigorously justified, typical fermionic momenta are smaller by λ_E. In practical terms, this separation allows one to approximate $\int d^2\mathbf{k}$ in the Eliashberg formula for the self-energy for a generic $\chi(q)$ by $2\pi N_F \int d\epsilon_{\mathbf{k}'} d\theta$, where $\mathbf{k}' = \mathbf{k} + \mathbf{q}$ and θ is the angle between $\mathbf{k}$ and $\mathbf{k}'$, with both set on the Fermi surface. Equation (3) then reduces to

$$\begin{aligned}\Sigma(\mathbf{k}, \omega_m) &= \Sigma(\omega_m) \\ &= i\tilde{g}^2 N_F \int \frac{d\Omega_n}{2\pi} \chi_L(\Omega_n) \int d\epsilon_{\mathbf{k}'} G(k', \omega_m + \Omega_n) \\ &= g^2 \int_0^{\omega_m} d\Omega_n \chi_L(\Omega_n),\end{aligned} \tag{18}$$

where we have defined $\chi_L(\Omega_n) = (1/2\pi) \int d\theta \chi(\Omega_n, \theta)$. For our choice of phonon propagator $\chi(q)$ this reduces to the Eliashberg result Eq. (13). On the real frequency axis, the

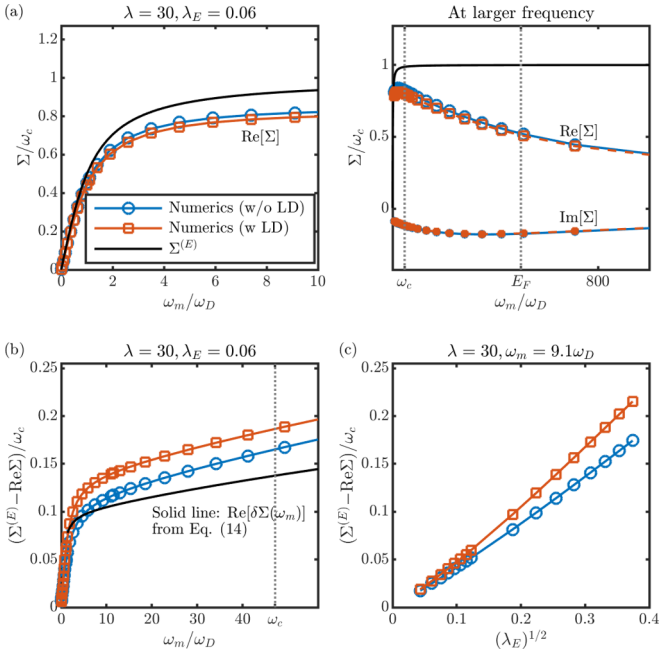

FIG. 3. One-loop electron self-energy for $E_F = 500\omega_D$, $\lambda_E = 0.06$, and $\lambda = 30$. (a) Numerical solution of the self-consistent equation (3) vs the perturbative expression $\Sigma^{(E)}(\omega_m)$ from Eq. (13). The numerical results obtained with and without Landau damping are shown as red and blue curves, respectively. The right panel in (a) displays the self-energy at larger frequencies, comparable to E_F. Both $\mathrm{Re}[\Sigma(\omega_m)]$ and $\mathrm{Im}[\Sigma(\omega_m)]$ evolve with frequency ($\mathrm{Im}[\Sigma(\omega_m)]$ is a constant at small ω_m and is not shown in the left panel). (b) A comparison between $\Sigma^{(E)}(\omega_m) - \mathrm{Re}[\Sigma(\omega_m)]$ and $\mathrm{Re}[\delta\Sigma(\omega_m)]$ from Eq. (14). (c) The verification of the scaling relation $(\Sigma^{(E)}(\omega_m) - \mathrm{Re}[\Sigma(\omega_m)])/\omega_D \propto \sqrt{\lambda_E}$ for an example $\omega_m/\omega_D \simeq 9$.

same consideration yields $\Sigma''(\omega) = -g^2 \int_0^\omega \chi_L''(\Omega) d\Omega$. In the literature, $g^2\chi_L''(\Omega)$ is often denoted $\alpha^2 F(\Omega)$ [7,59].

This analytical analysis of leading and subleading terms in the ME self-energy is supported by the numerical solution of the Eliashberg equations. The numerical results are obtained by solving the self-consistent equations iteratively, where the momentum integrations are carried out without making extra approximations. At frequencies below ω_D, $\Sigma(\omega_m)$ exhibits Fermi liquid behavior. The self-energy then saturates for an intermediate frequency range up to ω_c and eventually decreases at larger frequencies. We see that the imaginary part of $\Sigma(\omega_m)$ remains weakly frequency dependent up to $\omega_m \sim E_F$. The implication is that in the whole range $|\omega_m| \leqslant E_F$ it can be absorbed into the renormalization of the chemical potential. The difference between $\mathrm{Re}[\Sigma(\omega_m)]$ and the one-loop perturbative result $\Sigma^{(E)}(\omega_m)$ is shown in Fig. 3(b). The main contribution to this difference is captured by Eq. (14). In particular, we verified in Fig. 3(c) that, for $\omega_m > \omega_D$, $\mathrm{Re}[\Sigma(\omega_m)] - \Sigma^{(E)}(\omega_m)$ scales as $\lambda_E^{1/2}$, in agreement with Eq. (14).

C. Vertex corrections

The one-loop vertex correction is shown graphically in Fig. 4(a) and the associated two-loop self-energy with vertex renormalization is shown in Fig. 4(b). The relative strength of the two-loop self-energy compared to the one-loop one

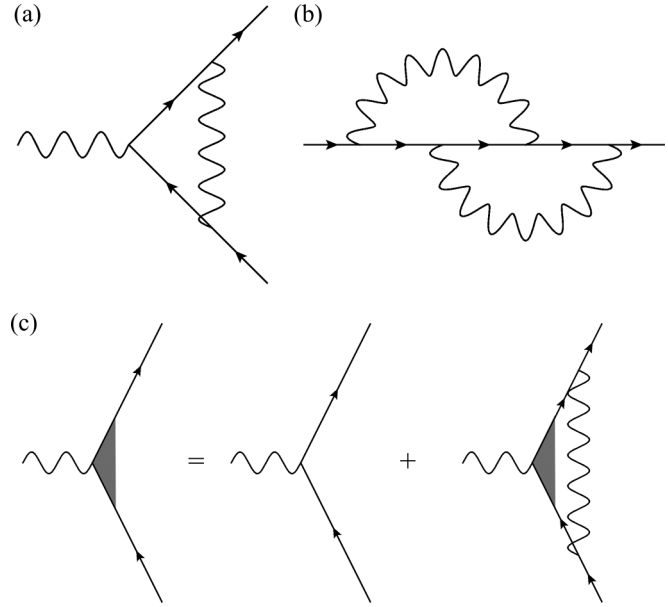

FIG. 4. Relevant diagrams: (a) one-loop vertex correction, (b) two-loop electron self-energy with vertex correction included, and (c) ladder series for the vertex.

determines the validity of Eliashberg theory. The one-loop vertex correction and the two-loop self-energy in 2D have been discussed previously in Ref. [8]. Here we reproduce earlier results and add additional details.

For external fermionic $k = (\mathbf{k}_F, \omega_m)$ and phononic $q = (\mathbf{q}, \Omega_n)$, the analytical expression for the one-loop correction to g is

$$\frac{\Delta g(k,q)}{g} = -i\frac{g^2}{2\pi}\int \frac{d\omega_m'}{(\omega_m - \omega_m')^2 + \omega_D^2}\int \frac{d\epsilon_{\mathbf{k}'}}{i\tilde{\Sigma}(\omega_m') - \epsilon_{\mathbf{k}'}} \times \frac{\mathrm{sgn}(\omega_m' + \Omega_n)}{\sqrt{(v_F|\mathbf{q}|)^2 + (\tilde{\Sigma}(\omega_m' + \Omega_n) + i(\epsilon_{\mathbf{k}'} + \mathbf{q}^2/2m))^2}}. \tag{19}$$

For $\mathbf{q} = 0$, the vertex correction *is not small* even if λ_E is small, as the full vertex function $g_{\mathrm{full}}(\omega_m, \Omega_n, \mathbf{q} = 0)$ must satisfy the Ward identity associated with the conservation of the total density:

$$\frac{g_{\mathrm{full}}(\omega_m, \Omega_n, \mathbf{q} = 0)}{g} = \frac{\tilde{\Sigma}(\omega_m + \Omega_n) - \tilde{\Sigma}(\omega_m)}{\Omega_n}. \tag{20}$$

At small ω_m, $\tilde{\Sigma}(\omega_m) \approx \omega_m(1 + \lambda)$; hence by the Ward identity we should have $g_{\mathrm{full}}(\omega_m, \Omega_n, \mathbf{q} = 0)/g = 1 + \lambda \gg 1$. We show below that this indeed holds. Putting $\mathbf{q} = 0$ in Eq. (19) and setting $\Omega_n > 0$ for definiteness, we perform the $\epsilon_{\mathbf{k}'}$ integration to obtain the one-loop vertex correction in the form

$$\frac{\Delta g(\omega_m, \Omega_n, \mathbf{q} = 0)}{g} = g^2 \int_{-\Omega_n}^{0} \frac{d\omega_m'}{(\omega_m - \omega_m')^2 + \omega_D^2} \times \frac{1}{\tilde{\Sigma}(\omega_m' + \Omega_n) - \tilde{\Sigma}(\omega_m')}. \tag{21}$$

For small $\omega_m, \Omega_n < \omega_D$, this gives $\Delta g(\omega_m, \Omega_n, \mathbf{q}=0)/g = \lambda/(1+\lambda)$, which approaches 1 in the strong coupling limit $\lambda \gg 1$. In this situation, we need to include higher-order vertex corrections. A simple experimentation shows that, at large λ, relevant diagrams for the full vertex $g_{\rm full}(\omega_m, \Omega_n, \mathbf{q}=0)$ form a ladder series, shown in Fig. 4. The corresponding integral equation at arbitrary ω_m and Ω_n is

$$\frac{g_{\rm full}(\omega_m, \Omega_n, \mathbf{q}=0)}{g} = 1 + g^2 \int_{-\Omega_n}^{0} \frac{d\omega'_m}{(\omega_m - \omega'_m)^2 + \omega_D^2} \times \frac{g_{\rm full}(\omega'_m, \Omega_n, \mathbf{q}=0)/g}{\tilde{\Sigma}(\omega'_m + \Omega_n) - \tilde{\Sigma}(\omega'_m)}. \quad (22)$$

For small $\omega_m, \Omega_n \ll \omega_D$, $g_{\rm full}(\omega_m, \Omega_n, \mathbf{q}=0) = g_{\rm full}(\mathbf{q}=0)$ is independent of frequency and Eq. (22) yields

$$g_{\rm full}(\mathbf{q}=0) = g + \frac{\lambda}{1+\lambda} g_{\rm full}(\mathbf{q}=0), \quad (23)$$

i.e., $g_{\rm full}(\mathbf{q}=0) = 1+\lambda$, consistent with the Ward identity.

Going beyond the low frequency limit, we note that $g_{\rm full}(\omega_m, \Omega_n, \mathbf{q}=0)$, given by (20), is the solution of Eq. (22) for arbitrary ω_m and Ω_n, i.e., the ladder series of vertex corrections reproduce the Ward identity associated with the conservation of the total density, no matter what ω_m and Ω_n are.

For $q \sim k_F$ the result is different. Integrating over $\epsilon_{\mathbf{k}'}$ in Eq. (19) in infinite limits we now obtain

$$\frac{\Delta g(k,q)}{g} = \frac{g^2}{2} \int d\omega'_m \frac{1 - \mathrm{sgn}(\omega'_m + \Omega_n)\mathrm{sgn}(\omega'_m)}{(\omega_m - \omega'_m)^2 + \omega_D^2} \times \frac{1}{\sqrt{(v_F q)^2 + (\tilde{\Sigma}(\omega'_m + \Omega_n) - \tilde{\Sigma}(\omega'_m) + iq^2/(2m))^2}} \quad (24)$$

$$\approx \frac{g^2}{4E_F \bar{q}\sqrt{1-\bar{q}^2}} \int d\omega'_m \frac{1 - \mathrm{sgn}(\omega'_m + \Omega_n)\mathrm{sgn}(\omega'_m)}{(\omega_m - \omega'_m)^2 + \omega_D^2}, \quad (25)$$

where $\bar{q} = |\mathbf{q}|/(2k_F)$. In the second line in (24) we have used the fact that $\tilde{\Sigma}(\omega'_m + \Omega_n) - \tilde{\Sigma}(\omega'_m)$ is much less than $v_F q$ or $q^2/2m$ for a generic $q \sim k_F$ and typical frequencies much smaller than E_F. Evaluating the remaining frequency integral, we find

$$\frac{\Delta g(k,q)}{g} = \frac{\lambda_E}{4\bar{q}} \frac{1}{\sqrt{1-\bar{q}^2}} \left[\arctan\left(\frac{\omega_m + \Omega_n}{\omega_D}\right) - \arctan\left(\frac{\omega_m}{\omega_D}\right) \right]. \quad (26)$$

We see that for generic $\omega_m \sim \Omega_n \sim \omega_D$, $\Delta g(k,q)/g \sim \lambda_E$, as long as $\bar{q}$ is not too close to either 0 or 1.

There is a caveat here: the vertex correction in Eq. (26) decreases at $\omega_m, \Omega_n > \omega_D$. On a more careful look, we found that this is an artifact of integrating over $\epsilon_{\mathbf{k}'}$ in Eq. (19) in infinite limits instead of introducing the lower cutoff at $-E_F$. Repeating the integration with this lower cutoff we find that, even at $\omega_m, \Omega_n > \omega_D$, the vertex correction remains of the form

$$\frac{\Delta g(k,q)}{g} = C(q) \frac{\lambda_E}{4} \frac{1}{\bar{q}\sqrt{1-\bar{q}^2}}, \quad (27)$$

where $C(q) = O(1)$.

We plot the one-loop vertex correction as a function of q and $\Omega_n \sim \omega_D$ in Fig. 5. We show the results obtained using both an infinite energy cutoff ($-\infty < \epsilon_{\mathbf{k}} < \infty$) and a finite energy cutoff ($-E_F < \epsilon_{\mathbf{k}} < \infty$). The two results for $\Delta g/g$ do differ, most notably at $|\mathbf{q}| \sim k_F$, but both remain of order λ_E for a generic $|\mathbf{q}|$.

We next substitute $\Delta g(k,q)$ into the two-loop diagram for the self-energy, Fig. 4(b). We label this contribution as $\Sigma^{(2)}(\omega_m)$. Analyzing the integral over phononic $\mathbf{q}$, we find that it is singular at $|\mathbf{q}|$ close to 0 and $2k_F$, where the vertex correction is enhanced, but the singularity is only logarithmic. Evaluating the full integral, we find, in agreement with Ref. [8],

$$\Sigma^{(2)}(\omega_m) \sim \lambda_E |\log \lambda_E| \Sigma^{(E)}(\omega_m). \quad (28)$$

We see that, as long as λ_E is small, the two-loop $\Sigma^{(2)}(\omega_m)$ is parametrically smaller than the Eliashberg self-energy, despite the fact that the integral comes from q where the vertex correction is singular. This singularity only accounts for $|\log \lambda_E|$ in the prefactor.

In Fig. 6 we present the result of numerical evaluation of $\Sigma^{(2)}(\omega_m)$ using an infinite cutoff in the integration over $\epsilon_{\mathbf{k}'}$. We see that the ratio $\Sigma^{(2)}/\Sigma^{(E)}$ is approximately constant at $\omega_m \leqslant \omega_D$ and as a function of λ_E does scale as $\lambda_E |\log \lambda_E|$. The drop of the ratio $\Sigma^{(2)}/\Sigma^{(E)}$ at larger frequencies is likely an artifact of an infinite cutoff. In any case, the ratio $\Sigma^{(2)}/\Sigma^{(E)}$ is small at small λ_E. For completeness we computed this ratio at $\lambda_E = 1$ and found that it still remains numerically small over the wide range of $\omega_D < \omega_m < E_F$ ($\Sigma^{(2)}/\Sigma^{(E)} \simeq 0.062$ at $\omega_m = \omega_D$).

For comparison with the Ising-nematic/Ising-ferromagnetic case below, we analyze how $\Delta g/g$ depends

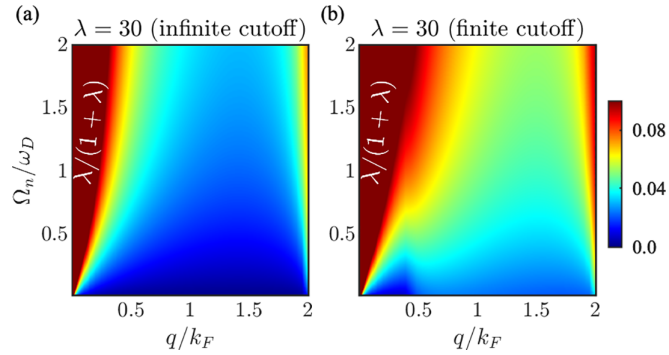

FIG. 5. Numerical results for one-loop vertex correction $\Delta g/g$ as a function of bosonic frequency Ω_n and momentum q for $\lambda = 30$, $\lambda_E = 0.06$, and external fermionic frequency $\omega_m = 0.1\omega_D$. Panels (a) and (b): the results of the calculations using infinite cutoff in the integration over dispersion, $-\infty < \epsilon_{\mathbf{k}} < \infty$, and a finite cutoff $-E_F < \epsilon_{\mathbf{k}} < \infty$, respectively. Note that vertex correction is large near $q = 0$ and also increases near $2k_F$, in agreement with our analytical treatment

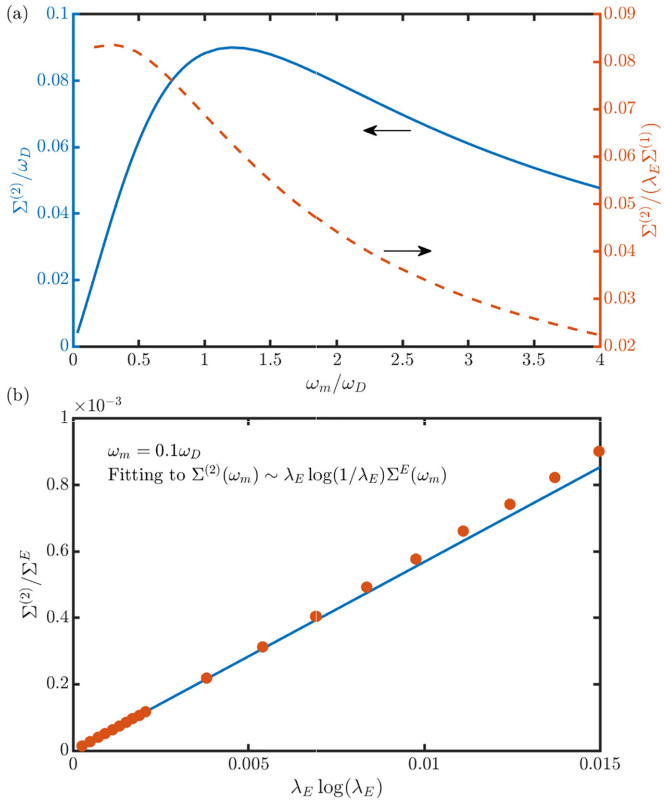

FIG. 6. (a) Blue line—the two-loop electron self-energy, obtained using infinite cutoff for integration over fermionic dispersion. The parameters are the same as in Fig. 3: $\lambda = 30$ and $\lambda_E = 0.06$. Brown line—the ratio $\Sigma^{(2)}/(\lambda_E\Sigma^{(E)})$. The ratio approaches a constant at $\omega_m \to 0$ and evolves at $\omega_m \sim \omega_D$. The drop of the ratio at larger ω_m is likely an artifact of using infinite cutoff for the integration over the dispersion. (b) Numerical verification of the scaling of $\Sigma^{(2)}(\omega_m)/\Sigma^{(E)}(\omega_m) \sim \lambda_E|\log\lambda_E|$ at small ω_m.

on characteristic momenta and frequencies. For definiteness we set $\mathbf{k} = \mathbf{k}_F$, $\Omega_n \sim \omega_D$ and vary ω_m, $q_\perp$, and $q_\parallel$, which are typical momentum components transverse and along the Fermi surface. At $\omega_D < \omega_m < \omega_c = (\pi/2)\lambda_E E_F$, where the self-energy $\Sigma(\omega_m)$ exceeds bare ω_m, we found after a simple experimentation

$$\frac{\Delta g(k,q)}{g} \sim \frac{\omega_c}{\omega_c + v_F q_\perp + \frac{q_\parallel^2}{2m}}. \tag{29}$$

Typical $v_F q_\perp$ are of order ω_c; typical $q_\parallel^2/(2m)$ are of order E_F. For these momenta,

$$\frac{\Delta g(k,q)}{g} \sim \frac{v_F q_\perp^{\rm typ}}{v_F q_\perp^{\rm typ} + \frac{(q_\parallel^{\rm typ})^2}{2m}}. \tag{30}$$

The "fast electrons/slow bosons" criterion requires typical $q_\perp$ to be much smaller than typical $q_\parallel$. This holds for $\lambda_E \ll 1$ because typical $q_\perp^{\rm typ} \sim \lambda_E k_F$, while $q_\parallel^{\rm typ} \sim k_F$. The strength of the vertex correction in Eq. (30) is, however, determined by the ratio of typical energies $v_F q_\perp^{\rm typ}/[(q_\parallel^{\rm typ})^2/2m]$ rather than typical momenta. In general, the ratios of typical energies and typical momenta are not the same, but in the electron-phonon case, $v_F q_\perp^{\rm typ}/[(q_\parallel^{\rm typ})^2/2m] \sim \lambda_E$ is the same as $q_\perp^{\rm typ}/q_\parallel^{\rm typ}$ because $q_\parallel^{\rm typ} \sim k_F$. As a consequence, the single parameter λ_E allows one to simplify the Eliashberg equations and keep vertex corrections small.

For larger ω_m, we found

$$\frac{\Delta g(k,q)}{g} \sim \frac{\omega_c}{\omega_m + v_F q_\perp^{\rm typ} + \frac{(q_\parallel^{\rm typ})^2}{2m}}. \tag{31}$$

Now typical $v_F q_\perp$ are of order ω_m, while typical $q_\parallel^2/(2m)$ are still of order E_F. For these momenta,

$$\frac{\Delta g(k,q)}{g} \sim \frac{\omega_c}{\omega_m + E_F} \sim \lambda_E \frac{1}{1 + \frac{\omega_m}{E_F}}. \tag{32}$$

We see that the vertex correction remains of order λ_E.

D. Summary of Sec. II

There are three energy scales in the electron-phonon problem: the bosonic energy ω_D, the dimension-full electron-phonon coupling g, and the Fermi energy E_F. This allows one to introduce two dimensionless ratios $\lambda = g^2/\omega_D^2$ and $\lambda_E = g^2/(E_F\omega_D) = \lambda\omega_D/E_F$. The latter is a small parameter for the Eliasberg theory. The strong coupling regime occurs at $\lambda \gg 1$, $\lambda_E \ll 1$. In this regime, the system displays Fermi liquid behavior at $\omega < \omega_D$, non-Fermi liquid behavior at $\omega_D < \omega_m < \omega_c$, with almost frequency independent $\Sigma(\omega_m) \approx \omega_c = (\pi/2)\lambda\omega_D = (\pi/2)\lambda_E E_F$, and Fermi-gas behavior at larger frequencies.

The three key results for the electron-phonon system, which we will later use for comparison with the behavior near a nematic QCP, are the following.

First, Eliashberg theory is rigorously justified even at strong coupling $\lambda \gg 1$, as long as the Eliashberg parameter $\lambda_E \ll 1$. The two-loop vertex correction to self-consistent one-loop Eliashberg theory is small in λ_E for all frequencies ω_m.

Second, the same small parameter λ_E also simplifies the calculations within Eliashberg theory: the Landau damping of phonons can be neglected in the calculation of the self-energy and the self-energy $\Sigma(\mathbf{k}, \omega_m)$ can be approximated by the local $\Sigma(\omega_m)$ and computed perturbatively rather than self-consistently. This holds for $\omega_m < E_F$. At larger ω_m, the fast electron/slow boson criterion is not valid and the Eliashberg equation (3) has to be reanalyzed.

Third, vertex corrections to Eliashberg theory become $O(1)$ at $\lambda_E = O(1)$ and become parametrically large at $\lambda_E > 1$, except for the smallest frequencies $\omega_m < \omega_D/\lambda_E$, where they remain small. Because $\lambda_E = g^2/(\omega_D E_F)$, this result implies that one cannot extend the Eliashberg theory of electron-phonon interaction to $\omega_D = 0$. For a finite E_F, Eliashberg theory is valid only when ω_D exceeds a certain value. At smaller ω_D, a new description is required.

We summarize the results for an electron-phonon system in Fig. 7.

III. QUANTUM CRITICAL METAL

We now analyze the validity of an Eliashberg-type description of a system of electrons interacting with soft collective bosons representing order parameter fluctuations. For

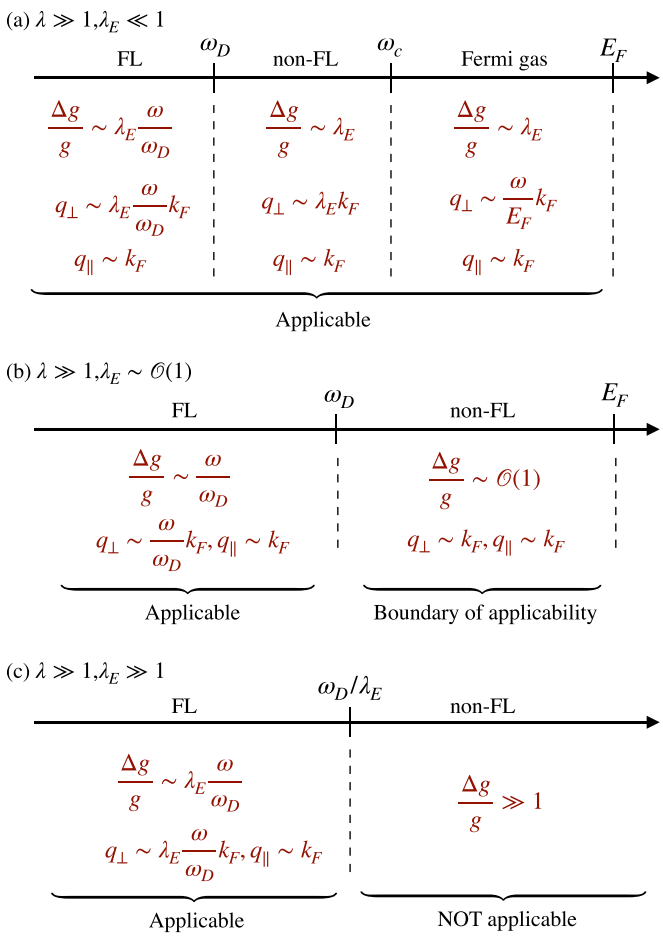

FIG. 7. Illustration of the applicability of Eliashberg theory for electron-phonon interactions at different energy scales: (a) $\lambda \gg 1$, $\lambda_E \ll 1$; (b) $\lambda \gg 1$, $\lambda_E \sim 1$; (c) $\lambda \gg 1$, $\lambda_E \gg 1$.

definiteness, we focus on the system near a $\mathbf{q} = 0$ Ising-ferromagnetic or Ising-nematic instability (see, e.g., Ref. [41] and references therein). The two cases differ by the form factor for fermion-boson coupling (it has d-wave form in the Ising-nematic case). We verified that the form factor does not play a critical role in our considerations and can be safely set to one (see also Ref. [39]). We do not consider the $SU(2)$ ferromagnetic case as the ordering transition there is affected by nonanalytic corrections to the spin susceptibility [60].

The set of Eliashberg-type equations is the same as Eqs. (3) and (4). Like for the electron-phonon case, it can be either derived diagrammatically [14,61] as self-consistent one-loop equations or obtained as stationary solutions of the Luttinger-Ward functional [41]. The bare fermionic Green's function is the same as in Eq. (2). For the bare bosonic propagator we choose the conventional Ornstein-Zernike form

$$\chi_0(\mathbf{q}) = \frac{D_0^*}{\xi^{-2} + |\mathbf{q}|^2}, \tag{33}$$

where D_0^* has dimension of mass^2 times energy and the propagator $\chi_0(q)$ has dimension of mass. We will define a related frequency scale $\omega_D^* = v_F \xi^{-1}$. The full generic $\chi_0(\mathbf{q})$ also contains a dynamical $(\Omega_n/v_F)^2$ term; however, this term only becomes relevant at frequencies above the upper limit of quantum-critical behavior (see below). For this reason, we neglect the Ω_n^2 term in χ_0 in our analysis.

For $\chi_0(q)$ given by (33), the fermion-boson coupling $\tilde{g}$ has the dimension of inverse mass. Accordingly, we introduce the effective interaction $g^* = \tilde{g}^2 D_0^*$ with dimensions of energy. Like in the electron-phonon case, there are three energy scales in this model: the effective coupling g^*, the bosonic energy ω_D^*, and the Fermi energy E_F. We again assume that E_F is the largest scale in the problem, i.e., set $E_F \gg \omega_D^*, g^*$. Like before, one can construct two dimensionless ratios out of these couplings. We choose them to be

$$\lambda^* = \frac{g^*}{4\pi\omega_D^*}, \quad \lambda_E^* = \frac{g^*}{E_F}. \tag{34}$$

By construction, $\lambda_E^* \ll 1$, but λ^* can be either small or large. We will see that the self-energy at the lowest ω_m is $\Sigma = \lambda^* \omega_m$, i.e., $\lambda^* \sim 1$ separates weak coupling ($\lambda^* < 1$) and strong coupling ($\lambda^* > 1$) regimes, respectively, analogous to λ for the electron-phonon interaction.

A. Solution of Eliashberg equations

The analysis of the Eliashberg equations for fermions near a $q = 0$ QCP has been done before in various contexts [11,19,32–39,41]. We list the existing results and present some new ones that will allow a direct comparison with the electron-phonon case.

We first discuss the calculation of the fermionic self-energy and bosonic polarization. Like for the electron-phonon case, we assume and then verify that the self-energy $\Sigma(k, \omega)$ can be approximated by a local $\Sigma(\omega_m)$. For such a self-energy, earlier calculations found that for $v_F|\mathbf{q}| \gg |\Omega_n|$, and both much smaller than E_F, the polarization can be written as a sum of static and dynamic terms $\Pi(\mathbf{q}, \Omega_n) = \Pi(\mathbf{q}, 0) + \delta\Pi(\mathbf{q}, \Omega_n)$, where $\delta\Pi(\mathbf{q}, \Omega_n)$ has the form of Landau damping:

$$\delta\Pi(\mathbf{q}, \Omega_n) = \frac{g^* k_F}{D_0^* \pi v_F^2} \frac{|\Omega_n|}{|\mathbf{q}|}. \tag{35}$$

This is similar to the electron-phonon polarization, Eq. (9) at $q \ll k_F$. Like there, the prefactor for the Landau damping term does not depend on the fermionic self-energy, i.e., Eq. (35) has the same form as for free fermions. We incorporate the static $\Pi(\mathbf{q}, 0)$ into $\chi_0(|\mathbf{q}|)$ by defining ξ as the renormalized correlation length and absorbing the velocity correction to the definition of D_0^*, like we did for the electron-phonon case. The full bosonic propagator reads

$$\chi(q) = \frac{D_0^*}{\xi^{-2} + |\mathbf{q}|^2 + \alpha \frac{|\Omega_n|}{|\mathbf{q}|}}, \tag{36}$$

where $\alpha = \frac{g^* k_F}{\pi v_F^2}$. Because relevant $\mathbf{q}$ are much smaller than k_F, the dynamical Landau damping term in $\chi(q)$ becomes relevant when Ω_n exceeds the scale

$$\omega^* = \frac{(\omega_D^*)^3}{g^* E_F} \sim \frac{\omega_c^*}{(\lambda^*)^3}, \tag{37}$$

where $\omega_c^* \sim E_F(\lambda_E^*)^2$ [the exact definition with the prefactor is in Eq. (42) below]. Because we consider λ_E^* to be small, we have $\omega_c^* \ll E_F$. We will see that, at strong coupling, when $\lambda^* > 1$, ω^* is the upper edge of Fermi liquid behavior, while

$\omega_c^* > \omega^*$ is the upper edge of quantum-critical non-Fermi liquid behavior. This identification implies that the Landau damping term in Eq. (36) is essential outside of the Fermi liquid regime. This distinguishes this case from the electron-phonon one, where the Landau damping term is irrelevant for all frequencies, as long as λ_E is small.

We now substitute $\chi(q)$ from Eq. (36) into the formula for the self-energy, Eq. (3). As before, we assume and verify that $\Sigma(\mathbf{k}, \omega_m) \approx \Sigma(\mathbf{k}_F, \omega_m) = \Sigma(\omega_m)$ with corrections controlled by the small parameter λ_E^*. The self-consistent equation for $\Sigma(\omega_m)$ is

$$\Sigma(\omega_m) = g^* \int \frac{d\Omega_n}{2\pi} \int \frac{d^2\mathbf{q}}{4\pi^2} \frac{1}{\xi^{-2} + |\mathbf{q}|^2 + \alpha \frac{|\Omega_n|}{|\mathbf{q}|}} \times \frac{1}{i\tilde{\Sigma}(\omega_m + \Omega_n) - \epsilon_{\mathbf{k}_F+\mathbf{q}}}, \tag{38}$$

where, as before, $\tilde{\Sigma}(\omega_m) = \omega_m + \Sigma(\omega_m)$. A straightforward analysis of the relevant scales in this equation shows that relevant $\Omega_n \sim \omega_m$, relevant $\epsilon_{\mathbf{k}_F+\mathbf{q}} \sim \tilde{\Sigma}(\omega_m)$, and relevant $|\mathbf{q}| \sim \xi^{-1}$ for $\omega_m < \omega^*$ and $|\mathbf{q}| \sim (\alpha|\omega_m|)^{1/3}$ for $\omega_m > \omega^*$. For the fermionic dispersion $\epsilon_{\mathbf{k}_F+\mathbf{q}}$ we will be using

$$\epsilon_{\mathbf{k}_F+\mathbf{q}} = v_F q_\perp + \frac{q_\parallel^2}{2m}, \tag{39}$$

where $q_\perp$ and $q_\parallel$ are momentum components perpendicular and parallel to the Fermi surface (along $\mathbf{k}_F$ and perpendicular to $\mathbf{k}_F$, respectively). Comparing relevant scales, we find (see below) that, for $\lambda_E^* \ll 1$, relevant $q_\parallel$ are much larger than $q_\perp$ as long as $\omega_m < \omega_{\max} \equiv (g^* E_F)^{1/2} \sim \omega_c^*/(\lambda_E^*)^{3/2} \sim E_F(\lambda_E^*)^{1/2}$. This indicates that the fast electrons/slow bosons condition is effectively realized even through the velocity of a bare boson is comparable with Fermi velocity. For frequencies below $\omega_{\max}$ we then can factorize the momentum integration, i.e., reexpress $d^2\mathbf{q}$ as $(1/v_F) d\epsilon_{\mathbf{k}_F+\mathbf{q}} dq_\parallel$ and integrate the fermionic propagator over $\epsilon_{\mathbf{k}_F+\mathbf{q}}$ and bosonic $\chi(|\mathbf{q}|, \Omega_n) \approx \chi(|q_\parallel|, \Omega_n)$ over $q_\parallel$. Using

$$\int \frac{d\epsilon}{i\tilde{\Sigma}(\omega_m + \Omega_n) - \epsilon} = -i\pi \, \mathrm{sgn}(\omega_m + \Omega_n), \tag{40}$$

we find that the right-hand side of Eq. (3) does not depend on the self-energy, i.e., has the same form as for free fermions. Completing the integration, we obtain

$$\Sigma^{(E)}(\omega_m) = \lambda^* \omega_m F\left(\frac{\omega_m}{\omega^*}\right), \tag{41}$$

where $F(x)$ is a crossover function. In the two limits $F(0) = 1$ and $F(x \gg 1) = [(4\pi)^{1/3}/\sqrt{3}]/x^{1/3}$. One can obtain the full analytical formula for $F(x)$, but it is rather cumbersome and not particularly enlightening so we do not present it here. We plot $\Sigma^{(E)}(\omega_m)$ in Fig. 8.

At small frequencies, $\Sigma^{(E)}(\omega_m)$ has the Fermi liquid form, $\Sigma^{(E)}(\omega_m) = \lambda^* \omega_m$. For large λ^*, $\Sigma^{(E)}(\omega_m) \gg \omega_m$. In this regime, relevant $q_\parallel \sim \xi^{-1}$, while relevant $q_\perp \sim (\omega_m/\omega^*)(\omega_D^*/E_F)\xi^{-1}$ are far smaller. In this regime we also have $q_\parallel^2/k_F \sim (\omega_D^*/E_F)\xi^{-1} \gg q_\perp$. This will be relevant to our analysis of vertex corrections below.

At larger $\omega_m > \omega^*$, the self-energy crosses over to a non-Fermi liquid, quantum-critical form $\Sigma^{(E)}(\omega_m) = \omega_m^{2/3}(\omega_c^*)^{1/3}$,

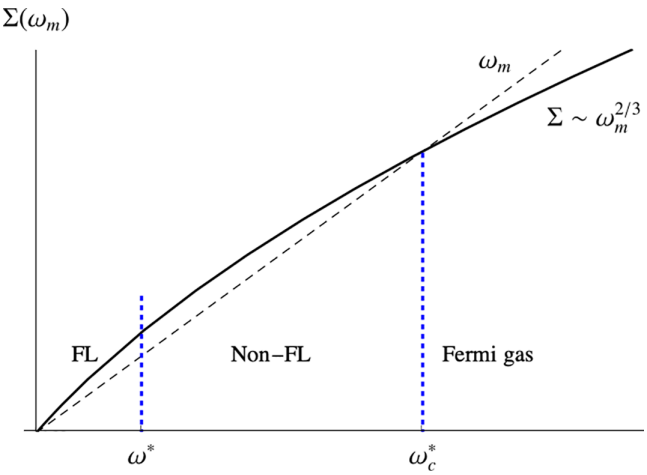

FIG. 8. One-loop perturbative Eliashberg self-energy $\Sigma^{(E)}(\omega_m)$ at $\lambda^* \gg 1$, but $\lambda_E^* \ll 1$. The self-energy is linear in ω_m for $\omega_m < \omega^*$ and crosses over to $\omega_m^{2/3}$ behavior at larger ω_m. It is larger than the bare ω_m for $\omega_m < \omega_c^*$, where $\omega_c^* \sim \omega^*(\lambda^*)^3 \gg \omega^*$. For $\omega_m < \omega^*$ the system is in the Fermi liquid regime. In between ω^* and ω_c^* it displays a non-Fermi liquid behavior. At larger ω_m the self-energy is smaller than ω_m and the system behaves as a Fermi gas.

where

$$\omega_c^* = \frac{1}{16\pi^2\sqrt{27}} \frac{(g^*)^2}{E_F} = \frac{1}{16\pi^2\sqrt{27}} E_F(\lambda_E^*)^2. \tag{42}$$

In terms of ω_c^*,

$$\omega^* = \frac{\sqrt{27}}{8} \frac{\omega_c^*}{(\lambda^*)^3}, \quad \omega_{\max} = 16\pi^2\sqrt{27} \frac{\omega_c^*}{(\lambda_E^*)^{3/2}}. \tag{43}$$

In the quantum-critical regime, relevant $q_\parallel \sim (\alpha\omega_m)^{1/3}$ and relevant $q_\perp \sim \omega_m^{2/3}\omega_0^{1/3}/v_F$. These can be reexpressed as $q_\parallel \sim k_F(\omega_m/\omega_c^*)^{1/3}\lambda_E^*$ and $q_\perp \sim k_F(\omega_m/\omega_c^*)^{2/3}(\lambda_E^*)^2$. We see that relevant $q_\parallel$ are again larger than $q_\perp$. However, relevant values of $q_\parallel^2/k_F$ are now comparable to relevant $q_\perp$. We will discuss below how this affects vertex corrections.

At even larger $\omega_m > \omega_c^*$, the self-energy becomes smaller than ω_m, although it still preserves its $\omega_m^{2/3}$ form. In this last regime relevant $q_\parallel \sim (\alpha\omega_m)^{1/3}$, like before, but relevant $q_\perp \sim \omega_m/v_F$. These can be reexpressed as $q_\parallel \sim k_F(\lambda_E^*)^{1/2}(\omega_m/\omega_{\max})^{1/3}$ and $q_\perp \sim k_F(\lambda_E^*)^{1/2}(\omega_m/\omega_{\max})$. The fast electrons/slow bosons criterion $q_\parallel \gg q_\perp$ is again satisfied, as long as $\omega_m < \omega_{\max}$. We label this frequency regime as "Fermi gas" as electrons in this regime behave almost like free particles.

At $\omega_m > \omega_{\max}$ the criterion of "fast electrons and slow bosons" is no longer valid and, as a result, one cannot factorize the momentum integration. In this regime, however, the Ω_n^2 term in the bare $\chi_0(q)$ cannot be neglected. We do not analyze this high-frequency regime here.

B. Subleading terms in the self-energy

As for the electron-phonon case, the corrections to the perturbative one-loop self-energy $\Sigma^{(E)}(\omega_m)$ come from (i) the momentum dependence of the static part $\Sigma(\mathbf{k}, 0)$, (ii) from nonfactorization of momentum integration, and (iii) from

keeping $\tilde{\Sigma}(\omega_m + \Omega_n)$ in the right-hand side of Eq. (38). The momentum dependent part of the self-energy is $\Sigma(\mathbf{k}, 0) \sim \epsilon_{\mathbf{k}}(8\lambda_E^*)^{1/2}$ [33]. It gives a small renormalization of the dispersion at $\lambda_E^* \ll 1$. The correction from nonfactorization of momentum integration is of the order of the ratio of relevant scales $(q_\perp/q_\parallel)^2$. In the quantum-critical regime this yields a relative correction to the self-energy of order $(\omega/\omega_c^*)^{2/3}(\lambda_E^*)^2$, which is at most $O((\lambda_E^*)^2)$. In the Fermi liquid regime, the correction is even smaller. In the Fermi gas regime the correction increases and becomes of order one at $\omega \sim \omega_{\max}$, which, we remind, is the largest frequency up to which the concept of fast electrons/slow bosons is applicable.

The correction $\delta\Sigma(\omega_m)$ from keeping $\tilde{\Sigma}(\omega_m + \Omega_n)$ is of order $\omega_m(\lambda_E)^{1/2}$ for all $\omega_m < \omega_{\max}$. We verified that it comes from internal $\Omega_n \sim \omega_{\max}$ and from $q_\perp \sim q_\parallel \sim k_F(\lambda_E^*)^{1/2}$. For such Ω_n, $\tilde{\Sigma}(\omega_m + \Omega_n) \approx \omega_m + \Omega_n$, i.e., the actual self-energy of an internal fermion is irrelevant. In explicit form we find

$$\delta\Sigma(\omega_m) = -\omega_m(\lambda_E)^{1/2} J, \tag{44}$$

where

$$J = \frac{1}{2\pi^2}\int_0^\infty dx \int_0^\infty dy \frac{x^2 y}{(4x^2+y^2)^{3/2}\left(x^3 + \frac{y}{4\pi}\right)} \approx 0.084 \tag{45}$$

and the integration variables are $x = q/[k_F(\lambda_E^*)^{1/2}]$ and $y = \Omega_n/\omega_{\max}$. We caution, however, that at $y = O(1)$, i.e., at $\Omega_n \sim \omega_{\max}$, the (Ω_n/v_F^2) term in $\chi(q)$, which we neglected, becomes comparable with the Landau damping and this may change the value of J. Still, it remains a number of order one and $\delta\Sigma(\omega_m)$ is much smaller than $\Sigma^{(E)}(\omega_m)$.

In Fig. 9, we show the numerical result for the self-energy for a small but finite λ_E^*. The solid line is $\Sigma^{(E)}(\omega_m)$ at $k = k_F$ and the blue squares are the full self-consistent numerical result $\Sigma(\omega_m) = \Sigma^{(E)}(\omega_m) + \delta\Sigma(\omega_m)$. In the limit $\lambda_E^* \to 0$, the full numerical $\Sigma(\omega_m)$ reduces $\Sigma^{(E)}(\omega_m)$, as expected. The difference, $\delta\Sigma(\omega_m)$, is linear in ω_m and the prefactor scales as $(\lambda_E^*)^{1/2}$, as in (44). The numerical data matches Eq. (44) very well.

C. Vertex correction

Vertex corrections to Eliashberg theory have been discussed in detail in [11,33]. We reproduce earlier results and present several new results below.

The lowest order vertex correction is given by the diagram in Fig. 4(a). In explicit form

$$\frac{\Delta g(k,q)}{g} = g^* \int \frac{d\Omega_n' d^2\mathbf{q}'}{(2\pi)^3} \frac{1}{i\tilde{\Sigma}(\omega_m + \Omega_n') - \epsilon_{\mathbf{k}+\mathbf{q}'}} \times \frac{1}{i\tilde{\Sigma}(\omega_m + \Omega_n' + \Omega_n) - \epsilon_{\mathbf{k}+\mathbf{q}'+\mathbf{q}}} \frac{1}{|\mathbf{q}'|^2 + \alpha\frac{|\Omega_n'|}{|\mathbf{q}'|}}, \tag{46}$$

where, we recall, $q = (\mathbf{q}, \Omega_n)$ is the external bosonic momentum and $k = (\mathbf{k}, \omega_m)$ is the external fermionic momentum.

Like for the electron-phonon case, the vertex correction at $\mathbf{q} = 0$ has to obey the Ward identity, Eq. (20), associated with the conservation of the particle number. We show that this indeed holds.

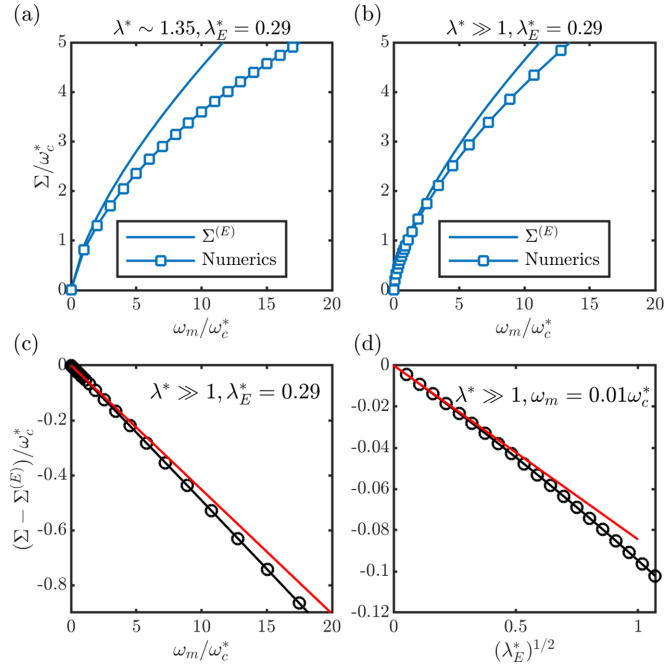

FIG. 9. Numerical results for the self-energy in Eliashberg theory for $\lambda_E^* = 0.29$ at (a) intermediate coupling $\lambda^* = 1.35$ and (b) infinitely strong coupling $\lambda^* = \infty$ at a QCP. The solid line is the perturbative expression $\Sigma^{(E)}$, Eq. (41), obtained by factorizing the momentum integration and squares are the numerical solutions of the full equation (38) for $\Sigma(\omega_m)$. (c) The difference between $\Sigma(\omega_m)$ and $\Sigma^{(E)}(\omega_m)$ at the QCP ($\lambda^* = \infty$). Red solid line is the analytic result, Eq. (44). (d) Verification of the scaling relation $\Sigma(\omega_m) - \Sigma^{(E)}(\omega_m) \propto (\lambda_E^*)^{1/2}$ (red line) at a particular ω_m.

In the Fermi liquid regime at $\omega_m < \omega^*$, an explicit calculation of $\Delta g(k, \Omega_n, \mathbf{q} = 0)/g$ yields

$$\frac{\Delta g(k, \Omega_n, \mathbf{q} = 0)}{g} = \frac{\lambda}{1+\lambda}. \tag{47}$$

At large λ, the one-loop vertex correction is close to one. To get the full vertex $g_{\text{full}}(k, \Omega_n, \mathbf{q} = 0)$ one has to sum the series of ladder vertex correction diagrams, just as we did for the electron-phonon case. The summation yields the expected result

$$\frac{g_{\text{full}}(k, \Omega_n, \mathbf{q} = 0)}{g} = \frac{1}{1 - \frac{\lambda}{1+\lambda}} = 1 + \lambda, \tag{48}$$

which is equal to $[\tilde{\Sigma}(\omega_m + \Omega_n) - \tilde{\Sigma}(\omega_m)]/\Omega_n$ in the FL frequency regime and thus satisfies the Ward identity, Eq. (20).

In the quantum-critical regime, the one-loop vertex correction is again of $O(1)$, but has a more complicated structure. Introducing dimensionless variables $x = \omega_m/\Omega_n$ and $x' = -(\omega_m + \Omega_n')/\Omega_n$ and setting both ω_m and Ω_n to be positive, we find the one-loop vertex correction in the form

$$\frac{\Delta g(x, \Omega_n)}{g} = \frac{2}{3}\int_0^1 \frac{dx'}{|x' - x|^{1/3}} \times \frac{1}{(1-x')^{2/3} + (x')^{2/3} + \left(\frac{\Omega_n}{\omega_c^*}\right)^{1/3}}. \tag{49}$$

The ladder series of vertex corrections in this situation can be reexpressed as an integral equation for $g_{\rm full}(x, \Omega_n)$:

$$g_{\rm full}(x, \Omega_n) = 1 + \frac{2}{3}\int_0^1 \frac{dx'}{|x'-x|^{1/3}} \frac{g_{\rm full}(x', \Omega_n)}{(1-x')^{2/3} + (x')^{2/3} + \left(\frac{\Omega_n}{\omega_c^*}\right)^{1/3}}. \tag{50}$$

This is an integral equation in the variable x, while Ω_n just acts as a parameter. One can easily verify that the solution of Eq. (50) is

$$g_{\rm full}(x, \Omega_n) = \left(\frac{\omega_c^*}{\Omega_n}\right)^{1/3}\left[(1-x)^{2/3} + x^{2/3} + \left(\frac{\Omega_n}{\omega_c^*}\right)^{1/3}\right]. \tag{51}$$

In the original variables, Eq. (51) explicitly reproduces the Ward identity, Eq. (20),

$$g_{\rm full}(\omega_m, \Omega_n) = 1 + \frac{[(\omega_m+\Omega_n)^{2/3} - (\omega_m)^{2/3}]\omega_0^{2/3}}{\Omega_n} = \frac{\tilde{\Sigma}(\omega_m+\Omega_n) - \tilde{\Sigma}(\omega_m)}{\Omega_n}. \tag{52}$$

For finite $\mathbf{q}$, the result is more involved. The one-loop vertex correction for $\mathbf{k}$ on the Fermi surface is a scaling function of five variables

$$\frac{\Delta g(k,q)}{g} = \Phi\left(\frac{\omega_m}{\Omega_n}, \frac{v_F q_\perp}{\tilde{\Sigma}(\omega_m)}, \frac{q_\parallel^2/2m}{\tilde{\Sigma}(\omega_m)}, \frac{\omega_m}{\tilde{\Sigma}(\omega_m)}, \frac{(\omega_D^*)^2}{E_F\tilde{\Sigma}(\omega_m)}\right). \tag{53}$$

In the Fermi liquid regime at $\omega_m < \omega^*$, typical $v_F q_\perp \sim \Sigma(\omega_m) = \lambda^*\omega_m$ and typical $(q_\parallel^2/2m)/\Sigma(\omega_m) \sim \omega^*/\omega_m$. We verified numerically that in this case Φ is of order $\omega_m/\omega^* \ll 1$, i.e., $\Delta g(k,q)/g \sim \omega_m/\omega^* \ll 1$.

In the quantum-critical regime the last two variables in Eq. (53) can be set to zero. The scaling function of the other three variables, $\Phi(x, y, z, 0, 0)$, is

$$\Phi(x,y,z,0,0) = \frac{3^{3/4}}{4\pi}\int_0^1 dr \int_0^\infty \frac{ds}{s^{3/2} + 3^{3/4}|r+x|} \times \left[\frac{1}{(1-r)^{2/3} + r^{2/3} + i(y+z+2\sqrt{|z|s})} + \frac{1}{(1-r)^{2/3} + r^{2/3} + i(y+z-2\sqrt{|z|s})}\right]. \tag{54}$$

The scaling function Φ in Eq. (54) is generally complex and can be parametrized as $\Phi = |\Phi|e^{i\psi_\Phi}$. We plot $|\Phi|$ and ψ_Φ in Fig. 10 for several values of parameters. We see that in general Φ is of order one, but not particularly close to one, in distinction to the case $q = 0$. In this situation, we expect that higher-order vertex corrections remain of order one, but do not change substantially the value of $\Delta g/g$ compared to the one-loop result.

Finally, in the Fermi gas regime $\omega_c^* < \omega_m < \omega_{\rm max}$, we have for typical $\mathbf{q}$, and $\Omega_n \sim \omega_D^*$, $q_\parallel^2/(2m)/\tilde{\Sigma}(\omega_m) \ll 1$, $(\omega_D^*)^2/[E_F\tilde{\Sigma}(\omega_m)] \ll 1$, $v_F q_\perp/\tilde{\Sigma}(\omega_m) \sim 1$, and $\omega_m/\tilde{\Sigma}(\omega_m) \approx 1$. In this situation, we find $\Phi \sim \Sigma(\omega_m)/\omega_m \sim (\omega_c^*/\omega)^{1/3} \ll 1$ and hence $\Delta g(k,q)/g \ll 1$.

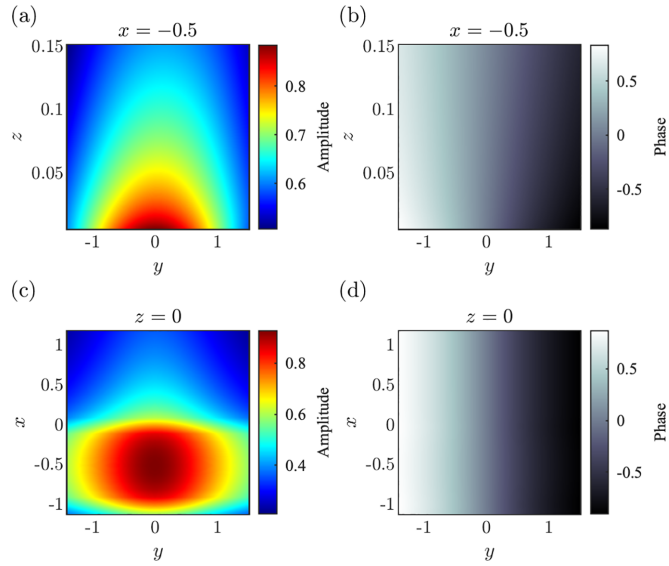

FIG. 10. Scaling function $\Phi(x, y, z, 0, 0) = |\Phi|e^{i\psi_\Phi}$, describing the one-loop vertex correction in the quantum-critical regime [cf. Eq. (54)]. The functions $|\Phi|$ and ψ_Φ are plotted in the (y, z) plane for $x = -0.5$ (a), (b) and in the (x, y) plane for $z = 0$ (c), (d).

For qualitative analysis we do the same as for the electron-phonon case and estimate $\Delta g(k,q)/g$ by using typical values of internal momenta and frequency. A simple experimentation shows that by order of magnitude

$$\frac{\Delta g(k,q)}{g} \sim \frac{\Sigma(\omega_m)}{\tilde{\Sigma}(\omega_n) + v_F q_\perp^{\rm typ} + \frac{(q_\parallel^{\rm typ})^2}{2m}}. \tag{55}$$

In the Fermi liquid and Fermi gas regimes the vertex correction is small because either $(q_\parallel^{\rm typ})^2/(2m) \gg \Sigma(\omega_m)$ or $\tilde{\Sigma}(\omega_n) \gg \Sigma(\omega_n)$. In the quantum-critical, non-Fermi liquid regime all parameters in Eq. (55) are of the same order and $\Delta g(k,q)/g$ is generally of order one, despite that typical $q_\parallel$ are much larger than typical $q_\perp$.

The quantitative measure of the strength of the vertex correction is the magnitude of the two-loop contribution to the self-energy with the vertex correction included, $\Sigma^{(2)}(\omega_m)$, compared to the one-loop $\Sigma^{(E)}(\omega_m)$. We show the corresponding diagram in Fig. 4(b). In the Fermi liquid and Fermi gas regimes, we find that $\Sigma^{(2)}(\omega_m) \ll \Sigma^{(E)}(\omega_m)$, consistent with the smallness of $\Delta g/g$. In the quantum-critical regime, earlier order of magnitude studies [11,33,47,48,62] have found that $\Sigma^{(2)}(\omega_m)$ is of the same order as $\Sigma^{(E)}(\omega_m)$, unless one extends the theory to large N or assumes that the prefactor for $q_\parallel^2$ in $\epsilon_{\mathbf{k}_F+\mathbf{q}}$ is much larger than v_F/k_F.

We confirmed these results, but went further and computed $\Sigma^{(2)}(\omega_m)$ numerically with the prefactor. We found

$$\Sigma^{(2)}(\omega_m) \simeq 0.038\Sigma^{(E)}(\omega_m). \tag{56}$$

We see that, while by order of magnitude $\Sigma^{(2)}(\omega_m)$ is comparable to $\Sigma^{(E)}(\omega_m)$, it is far smaller numerically. It has been argued [47–50,63] that self-energies with higher-loop order vertex corrections included contain logarithmic singularities.

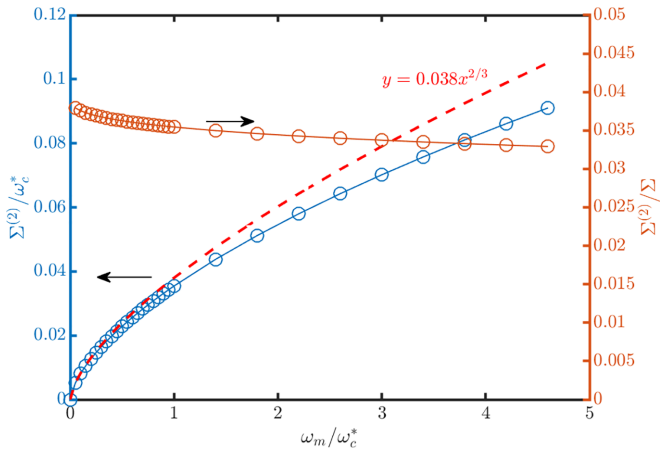

FIG. 11. Two-loop fermionic self-energy with vertex correction included, $\Sigma^{(2)}(\omega_m)$ [see Fig. 4(b)]. Left axis: $\Sigma^{(2)}(\omega_m)$ in units of the characteristic frequency ω_c^* (the upper edge of non-Fermi liquid behavior). Right axis: the ratio of $\Sigma^{(2)}(\omega_m)$ and the full one-loop Eliashberg self-energy $\Sigma(\omega_m) = \Sigma^{(E)}(\omega_m) + \delta\Sigma(\omega_m)$ (see Sec. III B).

We did not compute these terms explicitly, but based on Eq. (56) we expect them to contain small prefactors and remain small down to very small frequencies, before logarithmical singularities become relevant. We recall in this regard that the ground state near an Ising-nematic/Ising-ferromagnetic transition is a superconductor; hence in practice the behavior at the lowest frequencies is relevant only if for some reason superconductivity does not develop.

For completeness, we also present results at weak coupling, when both λ^* and λ_E^* are small. There are two weak coupling regimes: $\lambda^* \ll (\lambda_E^*)^{1/2} \ll 1$ and $(\lambda_E^*)^{1/2} \ll \lambda^* \ll 1$. We focus on the second regime as it borders the strong-coupling regime at $\lambda^* = O(1)$. In this regime, $\omega_c^* \ll \omega^*$, i.e., there is no range of non-Fermi liquid behavior, although the self-energy still interpolates between $\lambda^*\omega_m$ at small frequencies and $(\omega_m)^{2/3}(\omega_c^*)^{1/3}$ at higher frequencies (the relation between all characteristic frequencies is $\omega_c^* < \omega^* < \omega_D^* < \omega_{\max}$). A simple calculation shows that in this case typical $q_\perp^{\rm typ}$ are parametrically larger than $q_\parallel^{\rm typ}$ for all $\omega_m < \omega_{\max}$ [see Fig. 12(a) for their values] and the two-loop vertex correction is also small in λ^*. Hence Eliashberg theory is applicable and the self-energy within the theory can be computed within the perturbative one-loop approximation (See Fig. 11).

D. Summary of Sec. III

Like for the electron-phonon system, there are three energy scales in the problem: the bosonic energy ω_D^*, the coupling g^*, and the Fermi energy E_F. This allows one to introduce two dimensionless ratios $\lambda^* = g^*/(4\pi\omega_D^*)$ and $\lambda_E^* = g^*/E_F$. The latter is a small parameter in our theory. The strong coupling regime occurs at $\lambda^* > 1$. In this regime, the system displays Fermi liquid behavior at $\omega < \omega^* \sim \omega_D^*\lambda_E^*/(\lambda^*)^2$, quantum-critical, non-Fermi liquid behavior with $\Sigma(\omega_m) \propto \omega_m^{2/3}$ at $\omega^* < \omega_m < \omega_c^*$, where $\omega_c^* \sim g^*\lambda_E^*$, and Fermi-gas behavior at larger frequencies.

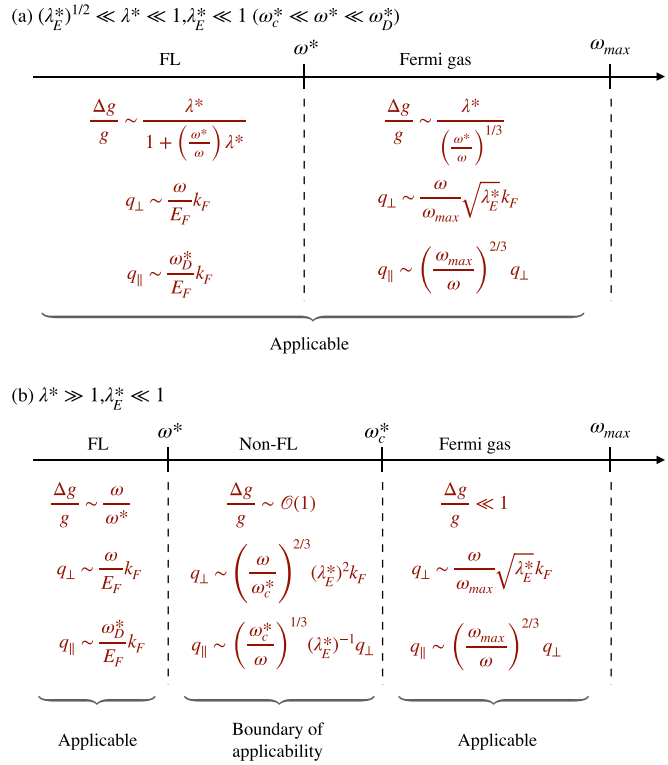

FIG. 12. Illustration of the applicability of Eliashberg theory near Ising-nematic/Ising-ferromagnetic critical point in a metal in (a) a weak coupling regime at some distance from a critical point and (b) a strong coupling regime near and at a critical point.

The three key results for the system near an Ising-nematic/Ising-ferromagnetic QCP are the following.

First, Eliashberg theory is rigorously justified at strong coupling $\lambda^* \gg 1$ in the Fermi liquid and Fermi gas regimes, but not in the quantum-critical regime. In the latter, the leading vertex correction is $O(1)$ even when λ_E^* is small. It is nevertheless small numerically, as evidenced by numerical smallness of the two-loop self-energy with vertex correction included.

Second, the small parameter λ_E^* simplifies the calculations within Eliashberg theory: the self-energy $\Sigma^{(E)}(\mathbf{k}, \omega_m)$ is well approximated by the local $\Sigma^{(E)}(\omega_m)$ and the momentum integration in the computation of $\Sigma^{(E)}(\omega_m)$ can be factorized by invoking the Migdal fast electron/slow boson criterion. This factorization is rigorously justified at all ω_m up to $\omega_{\max} \sim \omega_c^*/(\lambda_E^*)^{3/2} \gg \omega_c^*$. In this respect, λ_E^* plays the same role as λ_E for the electron-phonon case.

Third, and most important, the corrections to Eliashberg theory remain $O(1)$ (and numerically small) even at a QCP, where $\omega_D^* = 0$ and $\lambda^* = \infty$. In other words, Eliashberg theory near a nematic QCP, while not rigorously justified, is quite accurate numerically both near and at the QCP. Furthermore, the fast electron/slow boson criterion also remains valid at a QCP as long as λ_E^* is small, which allows one to simplify the calculations within Eliashberg theory.

We summarize the results for the Ising-nematic case in Fig. 12.

IV. CONCLUSIONS

In this paper we compared the validity of Eliashberg theory for electrons interacting with an Einstein phonon and with soft nematic fluctuations near an Ising-nematic QCP and soft magnetic fluctuations near an Ising-ferromagnetic QCP. Eliashberg theory is the set of coupled one-loop self-consistent equations for the fermionic self-energy and polarization operator, with vertex corrections neglected.

For electron-phonon interaction, Eliashberg theory has been justified by the argument that an Einstein phonon is a slow mode compared to a fermion (the effective boson velocity is smaller than the Fermi velocity). In the Ising-nematic/Ising-ferromagnetic case, this argument is not directly applicable as soft fluctuations are collective modes of electrons and their velocity is of the same order as v_F.

We examined self-consistent Eliashberg theory and two-loop corrections to it for both cases in the strong coupling regime, where the system displays Fermi liquid behavior at the lowest energies, non-Fermi liquid behavior in a wide range of intermediate energies, and Fermi gas behavior at the largest energies.

For the electron-phonon case, Eliashberg theory is rigorously justified when the Eliashberg parameter λ_E is small. Namely, the two-loop self-energy with vertex correction is small in λ_E. Simultaneously, using the same smallness of λ_E, the Eliashberg equations can be simplified into two decoupled perturbative one-loop equations, which can be easily solved. In physical terms, the smallness of λ_E follows directly from the condition that an Einstein phonon is a slow mode compared to electrons.

For the Ising-nematic/Ising-ferromagnetic case, soft bosons are collective modes of the electrons, and in the non-Fermi liquid quantum-critical regime there is no parametric smallness of the two-loop self-energy with vertex correction compared to the one-loop self-energy in the Eliashberg theory. Nevertheless, we found that the two-loop self-energy is numerically much smaller than the one-loop one. Additionally, the low-energy theory contains a small parameter λ_E^*, which plays the role of λ_E in the sense that it again allows one to reduce the coupled self-consistent one-loop Eliashberg equations to decoupled perturbative one-loop equations, which one can easily solve. The implication of these results is that Eliashberg theory for the Ising-nematic/Ising-ferromagnetic case is on rather solid grounds. It is very likely that this holds also for other cases when fermions interact with their soft collective excitations in the charge or spin channel.

There is one aspect in which the Eliashberg description of fermions coupled to soft collective bosons works even better than for fermions interacting with an Einstein phonon. Namely, for the collective boson case, the parameter λ_E^* is independent of the distance to a QCP and two-loop self-energy remains numerically smaller than the one-loop one even at a QCP. As a result, Eliashberg theory can be extended right to the QCP. For the electron-phonon case, the Eliashberg parameter λ_E^* is inversely proportional to the dressed Debye frequency and Eliashberg theory inevitably breaks down at some distance from the point where ω_D would vanish. Beyond this point, a completely new description in terms of polarons is needed [51–54,64].

ACKNOWLEDGMENTS

We thank Ar. Abanov, E. Berg, H. Goldman, R. Fernandes, M. Foster, I. Esterlis, P. A. Lee, D. Maslov, A. Millis, C. Murthy, S. Kivelson, A. Klein, P. Nosov, N. Prokofiev, S. Raghu, B. Svistunov, S. Sachdev, J. Schmalian, Y. Wang, and Y.-M. Wu for helpful discussions. The work of A. Ch. was supported by the U.S. Department of Energy, Office of Science, Basic Energy Sciences, under Award No. DE-SC0014402. Part of the work was done at the Kavli Institute for Theoretical Physics (KITP) in Santa Barbara, CA. KITP is supported by the National Science Foundation under Grants No. NSF PHY-1748958 and No. PHY-2309135.

[1] A. B. Migdal, Interaction between electrons and lattice vibrations in a normal metal, J. Exptl. Theoret. Phys. (U.S.S.R.) **34**, 1438 (1958) [Sov. Phys. JETP **7**, 996 (1958)].

[2] G. M. Éliashberg, Interactions between electrons and lattice vibrations in a superconductor, Zh. Eksp. Teor. Fiz. **38**, 966 (1960) [Sov. Phys. JETP **11**, 696 (1960)].

[3] P. B. Allen and R. C. Dynes, Transition temperature of strong-coupled superconductors reanalyzed, Phys. Rev. B **12**, 905 (1975).

[4] A. E. Karakozov, E. G. Maksimov, and S. A. Mashkov, Effect of the frequency dependence of the electron-phonon interaction spectral function on the thermodynamic properties of superconductors, Zh. Eksp. Teor. Fiz. **68**, 1937 (1975) [Sov. Phys. JETP **41**, 971 (1975)].

[5] F. Marsiglio and J. P. Carbotte, Gap function and density of states in the strong-coupling limit for an electron-boson system, Phys. Rev. B **43**, 5355 (1991); for more recent results see F. Marsiglio and J. P. Carbotte, Electron-phonon superconductivity, in *The Physics of Conventional and Unconventional Superconductors*, edited by Bennemann and Ketterson (Springer-Verlag, Berlin, 2006) and references therein.

[6] R. Combescot, Strong-coupling limit of Eliashberg theory, Phys. Rev. B **51**, 11625 (1995).

[7] F. Marsiglio, Eliashberg theory: A short review, Ann. Phys. (NY) **417**, 168102 (2020).

[8] A. V. Chubukov, A. Abanov, I. Esterlis, and S. A. Kivelson, Eliashberg theory of phonon-mediated superconductivity when it is valid and how it breaks down, Ann. Phys. (NY) **417**, 168190 (2020).

[9] J. M. Luttinger and J. C. Ward, Ground-state energy of a many-fermion system. II, Phys. Rev. **118**, 1417 (1960).

[10] A. J. Millis, Nearly antiferromagnetic Fermi liquids: An analytic Eliashberg approach, Phys. Rev. B **45**, 13047 (1992).

[11] B. L. Altshuler, L. B. Ioffe, and A. J. Millis, Low-energy properties of fermions with singular interactions, Phys. Rev. B **50**, 14048 (1994).

[12] B. L. Altshuler, L. B. Ioffe, A. I. Larkin, and A. J. Millis, Spin-density-wave transition in a two-dimensional spin liquid, Phys. Rev. B **52**, 4607 (1995).

[13] S. Sachdev, A. V. Chubukov, and A. Sokol, Crossover and scaling in a nearly antiferromagnetic Fermi liquid in two dimensions, Phys. Rev. B **51**, 14874 (1995).

[14] A. Abanov, A. V. Chubukov, and J. Schmalian, Quantum-critical theory of the spin-Fermion model and its application to cuprates: Normal state analysis, Adv. Phys. **52**, 119 (2003); Fingerprints of spin mediated pairing in cuprates, J. Electron Spectrosc. Relat. Phenom. **117–118**, 129 (2001).

[15] A. Abanov, A. V. Chubukov, and A. M. Finkel'stein, Coherent vs incoherent pairing in 2D systems near magnetic instability, Europhys. Lett. **54**, 488 (2001); A. Abanov and A. V. Chubukov, Spin-Fermion model near the quantum critical point: One-loop renormalization group results, Phys. Rev. Lett. **84**, 5608 (2000); A relation between the resonance neutron peak and arpes data in cuprates, **83**, 1652 (1999); A. Abanov, A. V. Chubukov, and M. R. Norman, Gap anisotropy and universal pairing scale in a spin-fluctuation model of cuprate superconductors, Phys. Rev. B **78**, 220507(R) (2008).

[16] S. Sachdev, M. A. Metlitski, Y. Qi, and C. Xu, Fluctuating spin density waves in metals, Phys. Rev. B **80**, 155129 (2009).

[17] E. G. Moon and S. Sachdev, Competition between spin density wave order and superconductivity in the underdoped cuprates, Phys. Rev. B **80**, 035117 (2009).

[18] N. E. Bonesteel, I. A. McDonald, and C. Nayak, Gauge fields and pairing in double-layer composite fermion metals, Phys. Rev. Lett. **77**, 3009 (1996).

[19] A. Abanov and A. V. Chubukov, Interplay between superconductivity and non-Fermi liquid at a quantum critical point in a metal. I. The γ model and its phase diagram at $T = 0$: The case $0 < \gamma < 1$, Phys. Rev. B **102**, 024524 (2020).

[20] Y. Wang and A. V. Chubukov, Superconductivity at the onset of spin-density-wave order in a metal, Phys. Rev. Lett. **110**, 127001 (2013).

[21] M. A. Metlitski and S. Sachdev, Quantum phase transitions of metals in two spatial dimensions. II. spin density wave order, Phys. Rev. B **82**, 075128 (2010).

[22] M. Vojta and S. Sachdev, Charge order, superconductivity, and a global phase diagram of doped antiferromagnets, Phys. Rev. Lett. **83**, 3916 (1999).

[23] K. B. Efetov, H. Meier, and C. Pepin, Pseudogap state near a quantum critical point, Nat. Phys. **9**, 442 (2013); H. Meier, C. Pépin, M. Einenkel, and K. B. Efetov, Cascade of phase transitions in the vicinity of a quantum critical point, Phys. Rev. B **89**, 195115 (2014); K. B. Efetov, Quantum criticality in two dimensions and marginal Fermi liquid, *ibid.* **91**, 045110 (2015).

[24] A. M. Tsvelik, Ladder physics in the spin Fermion model, Phys. Rev. B **95**, 201112(R) (2017).

[25] J. Bauer and S. Sachdev, Real-space Eliashberg approach to charge order of electrons coupled to dynamic antiferromagnetic fluctuations, Phys. Rev. B **92**, 085134 (2015).

[26] C. Castellani, C. Di Castro, and M. Grilli, Singular quasiparticle scattering in the proximity of charge instabilities, Phys. Rev. Lett. **75**, 4650 (1995); A. Perali, C. Castellani, C. Di Castro, and M. Grilli, d-wave superconductivity near charge instabilities, Phys. Rev. B **54**, 16216 (1996); S. Andergassen, S. Caprara, C. Di Castro, and M. Grilli, Anomalous isotopic effect near the charge-ordering quantum criticality, Phys. Rev. Lett. **87**, 056401 (2001).

[27] Y. Wang and A. V. Chubukov, Enhancement of superconductivity at the onset of charge-density-wave order in a metal, Phys. Rev. B **92**, 125108 (2015).

[28] D. Chowdhury and S. Sachdev, Density-wave instabilities of fractionalized Fermi liquids, Phys. Rev. B **90**, 245136 (2014).

[29] Z. Wang, W. Mao, and K. Bedell, Superconductivity near itinerant ferromagnetic quantum criticality, Phys. Rev. Lett. **87**, 257001 (2001); R. Roussev and A. J. Millis, Quantum critical effects on transition temperature of magnetically mediated p-wave superconductivity, Phys. Rev. B **63**, 140504(R) (2001); A. V. Chubukov, A. M. Finkel'stein, R. Haslinger, and D. K. Morr, First-order superconducting transition near a ferromagnetic quantum critical point, Phys. Rev. Lett. **90**, 077002 (2003).

[30] D. Dalidovich and S.-S. Lee, Perturbative non-Fermi liquids from dimensional regularization, Phys. Rev. B **88**, 245106 (2013).

[31] S. Lederer, Y. Schattner, E. Berg, and S. A. Kivelson, Enhancement of superconductivity near a nematic quantum critical point, Phys. Rev. Lett. **114**, 097001 (2015).

[32] P. A. Lee, Gauge field, Aharonov-Bohm flux, and high-T_c superconductivity, Phys. Rev. Lett. **63**, 680 (1989); B. Blok and H. Monien, Gauge theories of high-T_c superconductors, Phys. Rev. B **47**, 3454(R) (1993); C. Nayak and F. Wilczek, Non-Fermi liquid fixed point in 2 + 1 dimensions, Nucl. Phys. B **417**, 359 (1994); Y. B. Kim, A. Furusaki, X.-G. Wen, and P. A. Lee, Gauge-invariant response functions of fermions coupled to a gauge field, Phys. Rev. B **50**, 17917 (1994).

[33] J. Rech, C. Pépin, and A. V. Chubukov, Quantum critical behavior in itinerant electron systems: Eliashberg theory and instability of a ferromagnetic quantum critical point, Phys. Rev. B **74**, 195126 (2006).

[34] L. Dell'Anna and W. Metzner, Fermi surface fluctuations and single electron excitations near Pomeranchuk instability in two dimensions, Phys. Rev. B **73**, 045127 (2006); W. Metzner, D. Rohe, and S. Andergassen, Soft Fermi surfaces and breakdown of Fermi-liquid behavior, Phys. Rev. Lett. **91**, 066402 (2003).

[35] D. L. Maslov and A. V. Chubukov, Fermi liquid near Pomeranchuk quantum criticality, Phys. Rev. B **81**, 045110 (2010).

[36] Y. You, G. Y. Cho, and E. Fradkin, Nematic quantum phase transition of composite Fermi liquids in half-filled Landau levels and their geometric response, Phys. Rev. B **93**, 205401 (2016).

[37] I. Esterlis, H. Guo, A. A. Patel, and S. Sachdev, Large-N theory of critical Fermi surfaces, Phys. Rev. B **103**, 235129 (2021).

[38] Z. D. Shi, H. Goldman, D. V. Else, and T. Senthil, Gifts from anomalies: Exact results for Landau phase transitions in metals, SciPost Phys. **13**, 102 (2022).

[39] A. Klein, S. Lederer, D. Chowdhury, E. Berg, and A. Chubukov, Dynamical susceptibility of a near-critical nonconserved order parameter and quadrupole Raman response in Fe-based superconductors, Phys. Rev. B **98**, 041101(R) (2018); A. Klein, D. L. Maslov, L. P. Pitaevskii, and A. V. Chubukov, Collective modes near a Pomeranchuk instability in two dimensions, Phys. Rev. Res. **1**, 033134 (2019); A. Klein, A. V. Chubukov, Y. Schattner, and E. Berg, Normal state properties of quantum critical metals at finite temperature, Phys. Rev. X **10**, 031053 (2020); Y. Liu, W. Jiang, A. Klein, Y. Wang, K. Sun, A. V. Chubukov, and Z. Y. Meng, Dynamical exponent of a quantum critical itinerant

ferromagnet: A Monte Carlo study, Phys. Rev. B **105**, L041111 (2022).

[40] P. A. Nosov, I. S. Burmistrov, and S. Raghu, Interplay of superconductivity and localization near a two-dimensional ferromagnetic quantum critical point, Phys. Rev. B **107**, 144508 (2023).

[41] S.-S. Zhang, E. Berg, and A. V. Chubukov, Free energy and specific heat near a quantum critical point of a metal, Phys. Rev. B **107**, 144507 (2023).

[42] T. C. Wu, P. A. Lee, and M. S. Foster, Enhancement of superconductivity in a dirty marginal Fermi liquid, Phys. Rev. B **108**, 214506 (2023); P. A. Nosov, Y.-M. Wu, and S. Raghu, Entropy and De Haas–Van Alphen oscillations of a three-dimensional marginal Fermi liquid, *ibid.* **109**, 075107 (2024).

[43] Z. D. Shi, H. Goldman, Z. Dong, and T. Senthil, Excitonic quantum criticality: from bilayer graphene to narrow chern bands, arXiv:2402.12436.

[44] Y.-M. Wu, S.-S. Zhang, A. Abanov, and A. V. Chubukov, Interplay between superconductivity and non-Fermi liquid at a quantum critical point in a metal. IV. The γ model and its phase diagram at $1 < \gamma < 2$, Phys. Rev. B **103**, 024522 (2021).

[45] Y.-M. Wu, S.-S. Zhang, A. Abanov, and A. V. Chubukov, Interplay between superconductivity and non-Fermi liquid behavior at a quantum-critical point in a metal. V. The γ model and its phase diagram: The case $\gamma = 2$, Phys. Rev. B **103**, 184508 (2021).

[46] E. A. Yuzbashyan and B. L. Altshuler, Breakdown of the Migdal-Eliashberg theory and a theory of lattice-fermionic superfluidity, Phys. Rev. B **106**, 054518 (2022).

[47] M. A. Metlitski and S. Sachdev, Quantum phase transitions of metals in two spatial dimensions. I. Ising-nematic order, Phys. Rev. B **82**, 075127 (2010).

[48] S.-S. Lee, Low-energy effective theory of Fermi surface coupled with U(1) gauge field in $2 + 1$ dimensions, Phys. Rev. B **80**, 165102 (2009); Recent developments in non-Fermi liquid theory, Annu. Rev. Condens. Matter Phys. **9**, 227 (2018).

[49] T. Holder and W. Metzner, Fermion loops and improved power-counting in two-dimensional critical metals with singular forward scattering, Phys. Rev. B **92**, 245128 (2015).

[50] D. Pimenov, A. Kamenev, and A. V. Chubukov, One-dimensional scattering of two-dimensional fermions near quantum criticality, Phys. Rev. B **103**, 214519 (2021).

[51] A. S. Alexandrov, V. V. Kabanov, and D. K. Ray, From electron to small polaron: An exact cluster solution, Phys. Rev. B **49**, 9915 (1994).

[52] A. J. Millis, R. Mueller, and B. I. Shraiman, Fermi-liquid-to-polaron crossover. I. General results, Phys. Rev. B **54**, 5389 (1996).

[53] C. Zhang, N. V. Prokof'ev, and B. V. Svistunov, Bond bipolarons: Sign-free Monte Carlo approach, Phys. Rev. B **105**, L020501 (2022).

[54] J. Sous, C. Zhang, M. Berciu, D. R. Reichman, B. V. Svistunov, N. V. Prokof'ev, and A. J. Millis, Bipolaronic superconductivity out of a Coulomb gas, Phys. Rev. B **108**, L220502 (2023).

[55] S.-S. Zhang, Y.-M. Wu, A. Abanov, and A. V. Chubukov, Superconductivity out of a non-Fermi liquid: Free energy analysis, Phys. Rev. B **106**, 144513 (2022).

[56] A. Georges, O. Parcollet, and S. Sachdev, Quantum fluctuations of a nearly critical Heisenberg spin glass, Phys. Rev. B **63**, 134406 (2001).

[57] Y. Wang and A. V. Chubukov, Quantum phase transition in the Yukawa-Syk model, Phys. Rev. Res. **2**, 033084 (2020).

[58] F. Marsiglio, Phonon self-energy effects in Migdal-Eliashberg theory, arXiv:2101.12084.

[59] F. Marsiglio, Eliashberg theory in the weak-coupling limit, Phys. Rev. B **98**, 024523 (2018).

[60] A. V. Chubukov and D. L. Maslov, Spin conservation and Fermi liquid near a ferromagnetic quantum critical point, Phys. Rev. Lett. **103**, 216401 (2009).

[61] A. Klein and A. Chubukov, Superconductivity near a nematic quantum critical point: Interplay between hot and lukewarm regions, Phys. Rev. B **98**, 220501(R) (2018).

[62] A. V. Chubukov and D. V. Khveshchenko, Effect of Fermi surface curvature on low-energy properties of fermions with singular interactions, Phys. Rev. Lett. **97**, 226403 (2006).

[63] A. Eberlein, I. Mandal, and S. Sachdev, Hyperscaling violation at the Ising-nematic quantum critical point in two-dimensional metals, Phys. Rev. B **94**, 045133 (2016).

[64] C. Zhang, J. Sous, D. R. Reichman, M. Berciu, A. J. Millis, N. V. Prokof'ev, and B. V. Svistunov, Bipolaronic high-temperature superconductivity, Phys. Rev. X **13**, 011010 (2023).